The Super El Niño–Polar Vortex Paradox

QBO Modulation and a Testable Hypothesis for Winter 2026/27

M. C. TANYERİ
Independent Researcher, Istanbul, Türkiye
mcantanyeri@outlook.com

Abstract

The absence of a breakdown of the Arctic stratospheric polar vortex in the three strongest El Niño winters of the instrumental record (1982/83, 1997/98, 2015/16) poses an open question at the amplitude end of the canonical ENSO–stratosphere chain. Motivated by the El Niño developing during 2026, for which record-breaking values are forecast for October–December, this study re-examines that paradox in an exploratory framework using publicly available index series (ONI, RONI, NAO, AO, QBO; 1951–2026) and an event catalog derived from the NOAA SSW Compendium (1958–2024). Four results stand out. First, the ENSO–NAO relationship differs within the season: r=+0.21 for November–December and r=−0.12 for January–March. Both individual confidence intervals include zero, whereas the paired difference over the same winters excludes zero (Δr=+0.33; 95% CI +0.08/+0.56) and is preserved under a moving block bootstrap (L=3–8: +0.09/+0.54 to +0.13/+0.54). A single December–February mean (r=−0.04) can mask these opposing intraseasonal tendencies. Second, the seasonal-mean surface imprint of the QBO is close to zero (QBO50×AO r=−0.01), but the winter-based probability of an SSW appears higher in the easterly phase: the risk ratio is 1.26 (95% CI 0.75–2.12) under the November 50-hPa definition and 1.48 (0.94–2.32) in the 67-winter 30-hPa record; the value of 1.71 obtained with the DJF definition, which overlaps the outcome period, should be read as an upper bound. The ENSO×QBO interaction cannot be resolved with the present sample. In the continuous vortex regression the ONI-only model gives R^2=0.002, rising to R^2=0.126 once wQBO is added; this relationship rests on NCEP/NCAR Reanalysis-1, and its robustness across other reanalysis products has not yet been demonstrated. Third, all three super winters defined by ONI≥+2.0 occurred under wQBO and without an SSW; because n=3, this is a hypothesis-generating observational pattern rather than evidence. The 3/3 wQBO pattern is preserved under the 50-hPa November, November–December and DJF classifications and under 30-hPa November, but 1997/98 shifts to the easterly phase under 30-hPa DJF; a sequence-preserving permutation reference of 0.06–0.09 does not exclude chance. Under the RONI≥+2.0 ruler the cluster grows to four winters with the addition of 1991/92: 4/4 are SSW-free, but only 3/4 are wQBO. The QBO is therefore not a deterministic switch but a possible conditioner of uncertain magnitude. The observed ONI–U10 relationship (r=−0.17; p=0.16) and the segmented fit (ΔAIC=−0.3) provide no support for the vortex-level continuous signature of a simple saturation scenario; the planetary-wave forcing mechanism itself is not tested directly. Fourth, the European–Mediterranean end of the chain is tested directly with ERA5 in this revision (winters 1979/80–2021/22, n=43): a +1 standard deviation stronger vortex is associated with a positive-NAM-like 500-hPa geopotential height (Z500) anomaly pattern over the Atlantic–European sector, in which 36.6% of grid cells pass the BH-FDR (α=0.10) criterion, and with a DJF precipitation anomaly of −5.5 mm month^{-1} [95% CI −10.5/−0.8] in the Türkiye regional box (26–45°E, 36–42°N; a full-area mean that also includes ocean cells); the signs reverse for a weak vortex. The fraction of grid cells passing FDR for precipitation is low (1.5% in DJF), and when the fifteen regional coefficients are treated as a single family under BH-FDR none passes the threshold; the effect sizes are of order 7–12% of the regional climatologies, the regional signals disappear in the January–March window, and the U10 coefficient is erased by the inclusion of the NAO only in late winter. Winter 2026/27 is not a verdict on H1–H3 but an observational test in which prospectively defined conditional expectations will be updated against a new extreme observation.

Significance Statement

The intuition that "the warmer the Pacific, the harsher the European winter" is not a forecasting rule supported by the record. The absence of a major midwinter SSW in the three strongest El Niño winters measured to date is notable, but a causal or deterministic rule cannot be derived from three events. This study treats the QBO as one possible conditioner of that historical pattern: although the probability of an SSW appears higher in easterly-QBO winters under the main phase definitions, the effect size carries wide uncertainty. For Türkiye and the eastern Mediterranean, El Niño amplitude alone is likewise insufficient; the chain that should be monitored more directly is vortex evolution, downward coupling, the NAO/AO and Mediterranean circulation. In winters with a strong vortex the large-scale Atlantic–European circulation leans toward the state that relatively suppresses the southerly storm track carrying precipitation into the Mediterranean; with a weak vortex the sign reverses. In this revision that link is quantified for the first time with regional confidence intervals: the sign of the signal is consistent, its magnitude is modest, and the individual regional confidence intervals are fragile under multiple-comparison correction — a picture that supports neither a deterministic reading nor complete dismissal. The scientific value of 2026/27 lies not in proving or refuting a hypothesis in a single winter, but in showing how conditional expectations written before the outcome was known should be updated in the face of a new extreme event.

1. Introduction

As the summer of 2026 draws to a close, the equatorial Pacific is host to one of the most rapidly developing warm events of the instrumental era. The monthly Niño-3.4 anomaly reached +2.03 °C in July and the weekly value centered on 12 August reached +2.7 °C; subsurface heat content at 50–150 m locally exceeds +8 °C, forming an extraordinary energy reservoir. As of August 2026, NOAA CPC assigns a probability above 90% to the "very strong" category for autumn and winter; in the RONI measure adopted by that agency as its official index in February 2026, which removes tropical-mean warming, the October–December median forecast of +2.66 °C exceeds every event since 1950. The question is no longer whether the event will occur, but how the global teleconnection network — the atmospheric bridges that affect remote basins simultaneously — and the Northern Hemisphere stratosphere in particular will respond to forcing of this amplitude.

The canonical chain is well known. Strengthened convection in the central-eastern Pacific triggers a planetary-scale Rossby wave train that deepens the Aleutian Low, the semi-permanent low-pressure center of the North Pacific. This deepening interferes constructively with climatological stationary wave-1 — the largest-scale, geographically anchored persistent wave pattern of the atmosphere — and increases the upward wave activity directed into the stratosphere, the layer roughly 10–50 km above the weather-producing troposphere. When large-scale planetary waves generated in the troposphere reach the stratosphere, they transfer momentum to the westerly circulation around the pole and can decelerate the vortex; this transfer is termed planetary-wave forcing and weakens the polar vortex (PV) (Bell et al. 2009; Cagnazzo and Manzini 2009). The full chain is sketched in Figure 1.

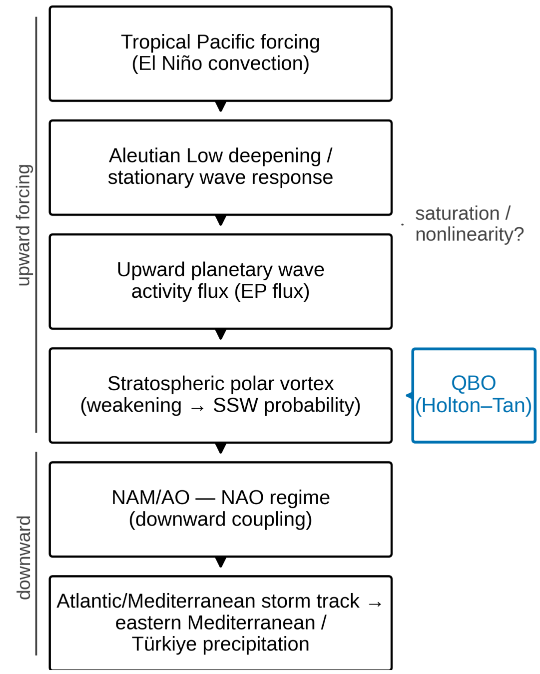

Figure 1. The canonical construction of the ENSO–stratosphere–Europe chain. The upward branch, running from tropical Pacific forcing to the Aleutian Low response and from there to the upward planetary wave activity flux and to vortex weakening / SSW probability, is drawn separately from the downward branch that descends through the NAM/AO–NAO regime to the Mediterranean storm track. Planetary waves carried along the upward branch transfer momentum to the westerly flow around the pole when they reach the stratosphere and can decelerate the vortex; the wave-activity box in the schematic represents this forcing. The box on the right marks the remote conditioning role of the QBO (Holton–Tan) acting on the vortex node, and the note on the left marks the saturation/nonlinearity question at the amplitude end of the forcing–response relationship. This is a conceptual schematic: it is not a composite map produced from numerical fields and cannot be used for quantitative interpretation (section 2.3).

If the weakening culminates in a major sudden stratospheric warming (SSW), a negative NAM/AO (Northern Annular Mode / Arctic Oscillation) signature descends into the troposphere over the following weeks (Baldwin and Dunkerton 2001), shifting the Atlantic storm track southward and increasing precipitation over the Mediterranean basin (Ineson and Scaife 2009; Domeisen et al. 2019; Zhang et al. 2024). The last link of this chain carries direct hydroclimatic significance for Türkiye: the strong negative relationship between winter precipitation and the NAO, especially for western Anatolia and the Marmara region, is among the most robust findings of the national literature (Türkeş and Erlat 2003, 2008; Baltacı et al. 2018).

Two remote controls that recur throughout this chain should be defined at the outset. The Quasi-Biennial Oscillation (QBO) is the oscillation of equatorial stratospheric winds between westerly (wQBO) and easterly (eQBO) phases with a mean period of about 28 months, and it remotely tunes the receptivity of the vortex to planetary waves arriving from below. The North Atlantic Oscillation

(NAO) and its close relative the Arctic Oscillation (AO) are the leading modes of variability of the Atlantic–European pressure distribution and set the latitude of the storm track: in the positive phase storms are directed toward northern Europe, in the negative phase toward the Mediterranean.

Findings that strain the textbook narrative have nevertheless accumulated at every link of the chain. SSW frequency does not increase in a way specific to El Niño but rises in both ENSO phases (Butler and Polvani 2011); Garfinkel et al. (2012a) explain this apparent paradox by the relative insulation from the ENSO teleconnection of the North Pacific region, where SSW precursors are most sensitive; and Palmeiro et al. (2023) expose the fragility of the observational basis by showing that the statistical significance of the difference between phases disappears in the 1950–2021 ERA5 record. The second complication concerns amplitude: the assumption that the stratospheric response grows linearly with forcing strength shows signs of saturation for extreme events (Zhou et al. 2019; Manzini et al. 2024), and and the observational record supports that doubt, since none of the three super El Niño winters experienced a major midwinter SSW and the vortex remained at record strength in 2015/16 (Ren et al. 2017). The third complication comes from the tropical stratosphere: the Holton–Tan effect (Holton and Tan 1980; Anstey and Shepherd 2014) weakens the vortex under easterly QBO, but both observational and modeling studies report that this modulation loses strength in El Niño winters (Wei et al. 2007; Garfinkel and Hartmann 2008; Calvo et al. 2009; Kumar et al. 2022). Fourth, the claim that the morphological type of an SSW (split or displacement) differentiates its surface signature is supported in reanalysis composites (Mitchell et al. 2013; Seviour et al. 2013; Hall et al. 2021) but dissolves beyond the first weeks in large model ensembles (Maycock and Hitchcock 2015; White et al. 2019, 2021; Lehtonen and Karpechko 2016).

The aim of this study is to combine these four lines of debate in a single framework, through the 2026/27 case and from an eastern Mediterranean perspective. The approach has two layers: published coefficients and composites are compiled with source verification, while the relationships that form the backbone of the claims are recomputed independently from publicly available series. This second layer addresses five questions: (i) to what extent is the intraseasonal structure of the ENSO–NAO relationship lost in single-season means; (ii) does the Holton–Tan effect live as a surface correlation or as a modulator of event probability, and how robust is that reading to the phase definition; (iii) can the absence of SSWs in super El Niño winters be explained by the QBO phase; (iv) does the saturation claim survive when it is tested with a continuous vortex measure instead of a binary SSW label; and (v) how large is the observational link between vortex strength and the European–Mediterranean circulation and Turkish winter climate when it is measured directly with grid-level FDR control and regional confidence intervals? In the eastern Mediterranean context we note that our search did not identify a direct, quantitative, station-scale literature linking vortex state to Turkish precipitation; as a first step toward closing that gap we compute the vortex–Türkiye link ourselves at the reanalysis scale (section 7.1) and explicitly leave station-scale verification as future work. The remainder of the paper is organized as follows: section 2 presents the data and methods; section 3 the ENSO–vortex pathway and nonlinearity; section 4 the QBO phases and the two faces of Holton–Tan; section 5 the QBO×ENSO interference and the super El Niño–wQBO coincidence; section 6 SSW typology; section 7 the European–Turkish teleconnections and the ERA5 test of the vortex–Türkiye link (section 7.1); section 8 the 2026/27 case; and section 9 discusses the results and the limits of prediction.

2. Data and Methods

2.1 Data

For the ENSO state we use the ERSSTv6-based ONI series of NOAA CPC (product: Seasonal ERSSTv6, centered base periods; file `oni.ascii.txt`; 1950–MJJ 2026); the complementary RONI series is taken from the same product family (Seasonal Relative ERSSTv6, 1991–2020 base period; file `RONI.ascii.txt`). Both files were downloaded on 28 August 2026 and archived as snapshots in the reproduction repository. Because peak ONI values can differ between ERSST versions, the three-winter set defined by the ≥+2.0 threshold is specific to the ERSSTv6 ruler; the threshold sensitivity analysis in Appendix A and the parallel RONI reporting test that dependence explicitly. For the NAO and AO we use the monthly CPC indices (1950–July 2026); these are the rotated-EOF and 1000-hPa height-EOF definitions, respectively, and they can differ from station-based alternatives (Hurrell; Gibraltar–Iceland) by ±0.05–0.1 at the level of correlation coefficients. Two series are used together for the QBO: the 50-hPa equatorial zonal-mean wind (NOAA CPC/CDAS, 1979–July 2026) and the 30-hPa equatorial zonal-mean wind (NOAA PSL, 1948–2026). The zonal-mean nature of these series reduces amplitudes relative to the Singapore station data (FUB/NASA) and can shift phase transitions by about one month; because our findings rest on the sign of the phase, this difference does not affect the results qualitatively, but it is taken explicitly into account in the discussion of the 2026/27 phase timing in section 8. The access date for all index series is 28 August 2026, and the product identification is repeated in every table and figure caption.

SSW events are taken from the NOAA CSL SSW Compendium (within the framework of Butler et al. 2015, 2017): a major SSW is defined by the reversal to easterlies of the 10-hPa, 60°N zonal-mean zonal wind during November–March (Charlton and Polvani 2007); central dates are taken with ERA5 priority and, for events absent from ERA5, from the JRA-55 and NCEP/NCAR columns. Because the Compendium ends in 2023, the events of 16 January and 4

March 2024 were added following Lee (2025) and are flagged explicitly in the tables. The Compendium's own ENSO and QBO labels are nowhere used in this study; all conditioning variables are derived from independent series (see section 2.2). The split/displacement classification is method-dependent — the zonal-mean criterion of Charlton and Polvani (2007) and the two-dimensional moment diagnostic of Mitchell et al. (2013) can assign different types for an appreciable fraction of borderline cases (for classification uncertainties see Baldwin et al. 2021) — so a type is assigned only to recent events for which there is broad agreement in the literature, with disputed cases marked by an asterisk. Vortex strength is computed as the DJF mean of the 10-hPa, 60°N zonal-mean zonal wind from NCEP/NCAR Reanalysis-1 (Kalnay et al. 1996; NOAA PSL THREDDS subsetting service; stratospheric values before 1958 should be read with caution).

Monthly ERA5 fields are used for the regional analysis (section 7.1) (Hersbach et al. 2020): 500-hPa geopotential height (Z500, m), total precipitation (mm month^{-1}) and 2-m temperature (K) are derived from the 1.5°, conservatively regridded ERA5 product in the WeatherBench2 archive (Rasp et al. 2024). Z500 and 2-m temperature are monthly means of 6-hourly steps; for precipitation, the 6-hourly accumulations of the WeatherBench2 variable total_precipitation_6hr were summed over each month and converted from meters of water equivalent to millimeters using a factor of 1000, giving monthly accumulated precipitation (mm month^{-1}). The extracted window is November 1978 – December 2022 and the domain is 80°W–50°E, 20–80°N; the access date is 29 August 2026. Coastlines are Natural Earth 50 m.

2.2 Definitions and statistics

"Winter Y" denotes the period from December of Y−1 through February of Y. The ENSO phase is defined by ONI_DJF (El Niño ≥ +0.5 °C, La Niña ≤ −0.5 °C); the operational "super" category of this study is ONI_DJF ≥ +2.0 °C, and the entire historical classification rests on that single measure. RONI, which removes tropical-mean warming, serves only as a complementary sensitivity ruler and as a characterization of the current 2026/27 context; the two indices are nowhere operated as interchangeable versions of the same threshold system. The effect of the threshold choice (≥+1.5, ≥+1.8, ≥+2.0) on the main pattern is presented in Appendix A (Table A1), and the catalog is additionally constructed with the RONI ruler (Table A2).

The QBO phase is defined with a pre-winter window so that the conditioning variable does not overlap the outcome period: the main classification is the sign of the November mean of the 50-hPa equatorial zonal-mean wind. The November–December and December–February classifications are reported as sensitivity analyses; in 41 of the 45 winters between 1980 and 2024 (91%) the November and DJF labels agree, the four that differ are transition winters (1983/84, 1986/87, 1992/93, 2017/18), and the November and November–December labels agree in 100% of cases. The warning that a single level may be insufficient (Dunkerton et al. 1988; Gray et al. 2018) is taken seriously: the entire classification was repeated for 30 hPa, and the November labels of the two levels agree in 35 of the 45 winters; the phase labels of pre-1979 winters come from the 30-hPa series alone. All QBO labels are derived from the wind series alone, independently of the SSW catalog. The continuous vortex analysis has two layers: the correlation and the segmented fit are constructed over the full 1959–2024 record (n=66), whereas the regression including the QBO is fitted by ordinary least squares to the joint sample in which ONI, U10–60N and the November 50-hPa phase are all available (n=45, 1980–2024). The nested models are U10 ~ ONI; U10 ~ ONI + wQBO; and U10 ~ ONI + wQBO + ONI×wQBO, and they are compared using R^2, adjusted R^2 and AIC.

Early winter is represented by the November–December window and late winter by January–March; this division is taken from the two-pathway literature (Ineson and Scaife 2009; Bell et al. 2009) and was not optimized against the data, although neither was it preregistered. The analysis framework is entirely exploratory: p values are reported not as confirmatory decision thresholds but as descriptive measures accompanying effect sizes and confidence intervals, and no multiple-comparison correction is applied in the index-layer analyses. Correlations are given as Pearson coefficients, with individual uncertainties as Fisher-z transformed 95% intervals; the early/late-winter correlation difference is bounded by a paired bootstrap in which the same winters are resampled (20 000 replicates) and is repeated with a moving block bootstrap (L=3, 5, 8) to guard against serial dependence. For winter-based SSW rates the outcome is always the binary "at least one major event within the winter"; cell uncertainties are given as Clopper–Pearson exact intervals, the effect size of the phase difference as a risk ratio with Fisher's exact test, and the ENSO×QBO interaction with Firth penalized logistic regression and a profile penalized likelihood ratio test. For the super El Niño–wQBO coincidence, the reference probability is computed with two randomizations that preserve the actual historical QBO phase sequence (circular shifting and three-winter block permutation); the naive value of 0.125, which assumes independence and equal phase frequency, is mentioned only for comparison. The assessment of the Türkiye-scale literature does not rest on a systematic search protocol but on the peer-reviewed sources accessible to the author, and statements of absence in the text are calibrated accordingly.

The regional ERA5 regression (section 7.1) implements the core of the design proposed in the Discussion of the second revision round and was carried out with the following setup. The sample comprises the winters 1979/80–2021/22 (n=43), and anomalies are relative to the 1991–2020 climatology. The predictor is the standardized DJF U10–60N (NCEP R1; section 2.1); the response fields were regressed separately in the DJF, November–December (ND) and

January–March (JFM) windows. Coefficient uncertainties are given as 95% percentile intervals from a winter-based bootstrap (B=5000; fixed seed); multiple comparisons over the grid domain are addressed with the Benjamini–Hochberg false discovery rate approach, and for the maps only the fraction of grid cells passing the BH-FDR (α=0.10) criterion is reported (Benjamini and Hochberg 1995; Wilks 2016). That fraction is descriptive and does not constitute a separate field-significance test. Regional effects are measured as area means over five boxes defined geographically without reference to the data: the Türkiye box (26–45°E, 36–42°N; 65 cells), Marmara (26–30.5°E, 39.5–42°N; 6 cells), the Aegean (26–30.5°E, 36.5–39.5°N; 6 cells), the Mediterranean coast (29.5–36.5°E, 36–37.5°N; 10 cells) and the eastern Mediterranean/Levant (25–37°E, 31–37°N; 32 cells). In all five boxes the average is a cosine-latitude-weighted full-area mean: no land–sea mask is applied and ocean cells are included in the average. This description was corrected during the reproducibility audit; the printed coefficients were verified to have been produced from unmasked full-area means, the methods text was corrected accordingly, and none of the numerical results changed. At 1.5° resolution these averages are coarse, and the "Türkiye box" is not a Türkiye average in the sense of administrative boundaries but a coarse 1.5° reanalysis box-area mean. The role of the NAO is assessed by comparing Model A (regional precipitation ~ U10s) with Model B (~ U10s + NAO) and by the bootstrap interval of the indirect component; this is an observational decomposition and not evidence of causal mediation. Regressing the ND window on the DJF predictor is partly acausal; for robustness each window was repeated with its own concurrent predictor version and the pattern correlations of the beta maps are reported (DJF 1.00, JFM 0.96, ND 0.68). Coefficients are per +1 standard deviation of U10 (strong vortex); for the weak-vortex reading the signs are reversed. Three windows × five regions form a single exploratory family of fifteen coefficients; when BH-FDR (α=0.10) is applied to that family no coefficient passes the threshold (smallest p=0.022) — individual 95% intervals that exclude zero should therefore be read as exploratory signals and not as findings that have passed family-level error control. A 0–60-day lagged design and station-scale verification (MGM/E-OBS) were deliberately left outside this revision and retained as future work.

2.3 A note on the figures

Figures 1–6 are conceptual schematics: they are not composite maps produced from numerical fields but script-drawn vector diagrams that convey the qualitative pattern of the data described in section 2.1 and of the cited literature composites (coastlines: Natural Earth 50 m). They cannot be used for quantitative interpretation, and this limitation is repeated in every caption. Figures 7–9 and Figure C1 are the exception to that rule: they are quantitative figures produced directly from the series and fields of section 2.1, and their captions give the data identification and the access date.

3. The ENSO–Vortex Pathway: Intraseasonal Structure and the Saturation Question

The first test of the canonical chain is whether the ENSO signature at the Atlantic end appears in a simple seasonal mean. Over 1951–2026 the correlation between ONI(DJF) and NAO(DJF) is −0.04 (Table 2a, row 1). When the winter is divided into intraseasonal windows, r=+0.21 in early winter (November–December; 95% CI −0.01/+0.42; p=0.06) and r=−0.12 in late winter (January–March; 95% CI −0.33/+0.11). Both individual relationships are weak and their confidence intervals include zero. By contrast, a paired bootstrap over the same winters gives Δr=+0.33 with a 95% CI of +0.08/+0.56 for the difference between the windows. The result is preserved under the moving block bootstrap: +0.09/+0.54 for L=3, +0.11/+0.53 for L=5 and +0.13/+0.54 for L=8. What is strong, therefore, is not the individual early- or late-winter correlations but the systematic differentiation between the two windows. This pattern is consistent with the two-pathway literature but is not by itself evidence of a causal pathway. The methodological inference is narrower and more robust: a single DJF mean can render the ENSO–NAO relationship invisible by adding together opposing intraseasonal tendencies.

Composites show the same structure at the event level. Across twenty-five El Niño winters the NAO falls from a November–December mean of +0.33 to +0.02 in January–March; restricted to strong events (ONI ≥ +1.5; n=7) the decline runs from +0.69 to +0.29 and the late-winter AO mean reaches −0.28. An important qualification is that the composite shows a weakening rather than a full sign reversal. The reversal is event-dependent, with clear examples — from +0.42 to −1.19 in 1957/58, from +1.64 to −0.58 in 1986/87 and from +0.77 to −0.34 in 1979/80 — but 2015/16 spent the entire winter on the positive side (+1.99 → +0.81). Geng et al. (2017) show that the abrupt early-January reversal in super events can arise, independently of the stratosphere, from the interaction of the event with the annual cycle of the subtropical jet; the spread in our composite implies that this mechanism does not operate with the same strength in every event. The qualitative counterpart of the early- and late-winter regimes is given in Figure 2.

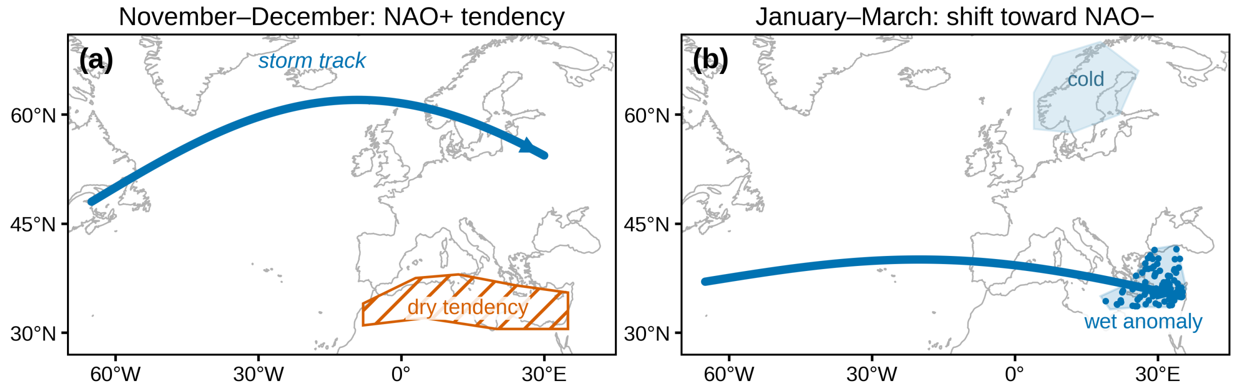

Figure 2. Intraseasonal sign asymmetry of the North Atlantic response in El Niño winters. (a) November–December: a tendency toward NAO+, a northward-shifted storm track and a dry-signed anomaly over the Mediterranean. (b) January–March: a shift toward NAO−, a southward-displaced flow, wet-signed anomalies over the eastern Mediterranean and cold-signed anomalies over northern Europe. The patterns are a qualitative summary of the correlations reported in section 3 and of the cited literature composites. This is a conceptual schematic: it is not a composite map produced from numerical fields and cannot be used for quantitative interpretation (section 2.3).

SSW frequency is the second test of the chain. In the 1958–2024 record there are 7.9 major SSWs per 10 phase-winters in El Niño winters, 7.4 in La Niña winters and 5.5 in neutral winters; these values are not event rates per chronological decade but descriptive event densities scaled by the number of phase-winters. On a winter basis, the fractions of winters with at least one major SSW are 58%, 65% and 45%, respectively (Table 3a). Both ENSO phases therefore show higher fractions than neutral winters, while the El Niño–La Niña difference is small. Read together with the higher ENSO-phase frequencies of Butler and Polvani (2011) and the longer-record analysis of Palmeiro et al. (2023), which finds no discriminating difference between phases, this result underlines the importance of period and classification sensitivity; our own numbers are consistent with the phase-symmetry explanation of Garfinkel et al. (2012a).

The weakest link of the chain is the amplitude assumption. In the three winters with the largest forcing — 1982/83, 1997/98 and 2015/16, the peaks of the catalog (Table 1) — there is no major midwinter SSW, and in 2015/16 the vortex remained at record strength (Ren et al. 2017). Zhou et al. (2019) offer a physical candidate for saturation: in extreme events the westward expansion of convection toward the Maritime Continent disrupts the constructive interference of the anomalous wave train with climatological wave-1, so the forcing grows while its effective projection does not. Manzini et al. (2024), by contrast, report that the El Niño branch remains approximately linear in the model world. This debate arrives at an unexpected place when it is tested with a continuous vortex measure rather than a binary SSW label, and it is taken up at the end of section 5; section 5 also adds a third candidate explanation for the absence of SSWs in the record, namely the QBO phase.

4. The Two Faces of Holton–Tan: A Dead Correlation and a Live Probability

The stratospheric body of the Holton–Tan effect is not in dispute: in easterly-QBO winters the vortex is weaker than under westerly QBO by more than 10 m s^{-1} at 10 hPa (Holton and Tan 1980; Anstey and Shepherd 2014; Watson and Gray 2014), and the relationship is strongest when it is defined near 50 hPa — Watson and Gray (2014) justify that choice by the correlation of 0.58 between the November–February equatorial wind and the 60°N/10-hPa wind, whereas Dunkerton et al. (1988) and Gray et al. (2018) argue that the deep phase profile rather than a single level is decisive. On the mechanism side, the classical zero-wind-line/waveguide account competes with the secondary meridional circulation of the QBO, and idealized experiments favor the latter (Garfinkel et al. 2012b; Watson and Gray 2014). It is also known that the effect is strong in early winter and weakens, or even changes sign, in late winter (Lu et al. 2020). The opposing effects of the two phases on the waveguide are shown in Figure 3.

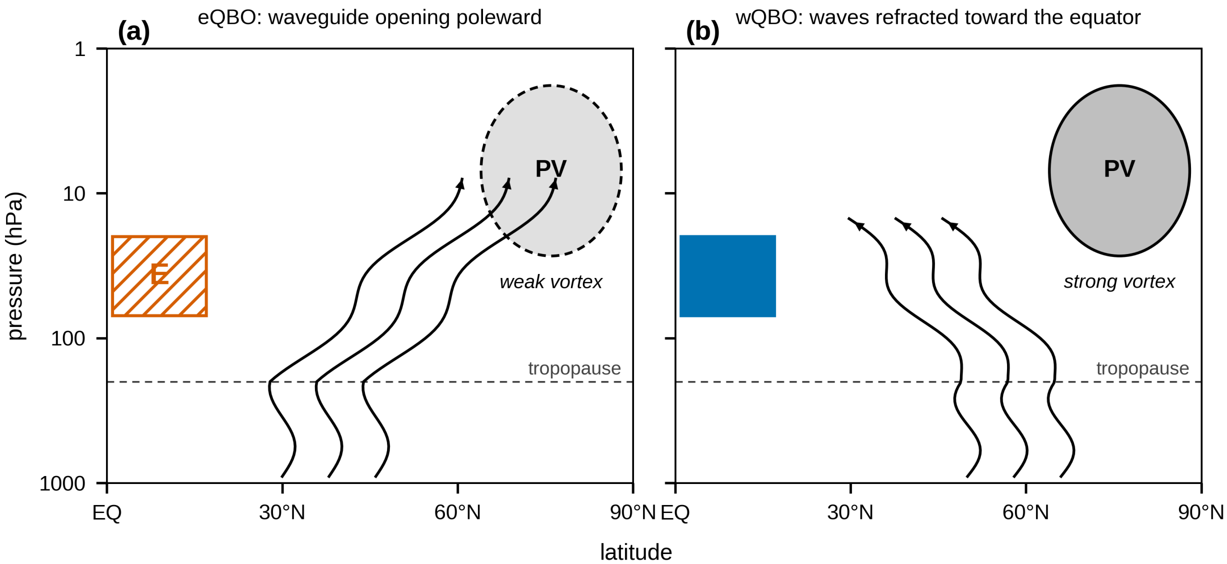

Figure 3. The waveguide interpretation of the Holton–Tan mechanism. (a) Under easterly QBO the equatorial easterly layer forms a critical line that directs planetary waves poleward and leaves the vortex more exposed to wave forcing. (b) Under westerly QBO the waves refract toward the equator and the vortex is relatively protected. The pressure axis is logarithmic; PV denotes the polar vortex and the dashed outline a weakened vortex. This is a conceptual schematic: it is not a composite map produced from numerical fields and cannot be used for quantitative interpretation (section 2.3).

At the surface, by contrast, the effect either disappears or becomes apparent depending on the measurement language, and that duality is the second main finding of this paper. In the language of seasonal-mean correlation there is no trace: r=−0.01 between QBO50(November–December) and AO(DJF) (n=47), and +0.06 for QBO30 (n=76); the phase composites are likewise not discriminating (AO mean −0.03 in the W phase and −0.01 in the E phase; Table 2a, rows 6–8).

In the language of events the trace becomes visible, but its precision is sensitive to the phase definition, and that sensitivity was underestimated in the first version of this paper. Under the pre-winter definition (November 50 hPa; 1980–2024), 63% of easterly-QBO winters see at least one major SSW against 50% of westerly-QBO winters (12/19 versus 13/26); the risk ratio is 1.26 (95% CI 0.75–2.12; Fisher's exact test p=0.545). When the same calculation is built on the DJF mean the fractions become 71% and 42% and the risk ratio rises to 1.71 (0.99–2.96; p=0.071) — but because this definition overlaps the conditioning variable with the outcome period it should be read as an upper bound. The single continuous series that extends the sample to 67 winters (30 hPa, 1958–2024) falls between the two: 67% versus 45%, risk ratio 1.48 (0.94–2.32; p=0.089). What the three definitions share is the constancy of the direction; their common weakness is that the confidence intervals include unity (Table 3b; Figure 8a). The Holton–Tan effect therefore reaches the surface not as a seasonal-mean correlation but as a shift in event probability whose magnitude is estimated in the 1.3–1.5 range and cannot be pinned down with the present sample.

The contradiction between the two languages is only apparent, and its resolution lies in the sparseness of stratosphere–troposphere coupling: only about half of SSWs bring the canonical negative-NAM signature down to the surface (Karpechko et al. 2017; Baldwin et al. 2021), and once the signal of those that do descend is diluted in the same seasonal mean by those that do not and by SSW-free winters, the correlation evaporates. Holton–Tan is not a surface correlation but a modulator of event probability. This reading is consistent both with the composite-based surface signature of Marshall and Scaife (2009) and with the QBO being a genuine source of skill in ensemble-mean seasonal forecasting (Scaife et al. 2014; the Atlantic imprint known since Ebdon 1975): predictability comes not from the raw index correlation but from the distillation of a probability shift within an ensemble.

5. QBO × ENSO Interference and the Super El Niño–wQBO Coincidence

When the two modulators are superposed the interaction is not linear. The observational and modeling literature converges on the finding that the Holton–Tan modulation remains strong in La Niña winters and weak in El Niño winters (Wei et al. 2007; Garfinkel and Hartmann 2008; Calvo et al. 2009; Richter et al. 2011); Kumar et al. (2022) further strain the assumption of pure additivity by showing that westerly QBO and El Niño can interfere constructively over the Aleutian Low.

The present analysis can neither confirm nor exclude that picture. When the winter-based risk table (Table 3c) is built with the pre-winter November 50-hPa phase and the 1980–2024 record, the eQBO and wQBO cells give the same fraction in El Niño winters (3/6 and 5/10; both 0.50). The difference appears larger in neutral winters (4/7 versus 1/6), but the cells are limited to six or seven winters. When the 30-hPa November phase and the 67-winter record are used, the

El Niño cells separate again (eQBO 9/13=0.69; wQBO 5/11=0.45). In the Firth penalized logistic model the interaction term has an odds ratio of 0.47 in the short record (95% CI 0.04–5.96; p=0.541) and 1.13 in the long record (0.14–8.92; p=0.904). Because the point estimates change with the definition and the intervals are wide, neither the direction nor the magnitude of the ENSO×QBO interaction can be resolved with the present observational sample.

The continuous vortex measure provides different information, but it does not measure the saturation mechanism itself. Across the 66 winters between 1959 and 2024 the relationship between ONI and the DJF mean U10–60N is weak and consistent with zero (r=−0.17; p=0.16; slope −1.6 m s^{-1} °C^{-1}); for RONI, r=−0.16. Although the best break in the segmented fit is found at +1.6 °C, model selection does not support a break (ΔAIC=−0.3; Figure 7). This result provides no observational support for the continuous signature expected at the polar vortex level under a simple saturation scenario, and it is not a direct test of the proposed convection → wave-1 interference → upward wave flux mechanism. The three super winters fall at the 21st, 76th and 97th percentiles of the U10 distribution and are therefore not homogeneous in continuous vortex strength. In the joint sample (n=45; 1980–2024) the ONI-only model gives R^2=0.002 (adjusted R^2=−0.02; ONI coefficient −0.37 m s^{-1} °C^{-1}, 95% CI −3.14/+2.40, p=0.79). When the wQBO indicator is added, R^2 rises to 0.126 (adjusted R^2=0.085; ΔAIC=−4.0) and wQBO is associated with a vortex stronger by +6.79 m s^{-1} (95% CI +1.19/+12.39; p=0.019). The ENSO×QBO term adds only 0.005 to R^2, has a coefficient of −1.25 m s^{-1} °C^{-1} (95% CI −6.83/+4.33; p=0.65) and worsens the AIC (ΔAIC=+1.8). The QBO here is not a deterministic switch but a conditioner that is more visible than ENSO amplitude in the present sample and yet limited. This regression rests on NCEP/NCAR Reanalysis-1; independent reanalysis verification of the coefficient magnitude and of the super-winter percentiles with ERA5 and, if possible, JRA-55 has not yet been carried out (for the R1–R2 comparison bearing on the product dependence of the 10-hPa predictor see section 9).

On this basis the most prominent pattern in the catalog should be read with the distinction between evidence and pattern preserved. All three winters with ONI≥+2.0 — 1982/83, 1997/98 and 2015/16 — coincided with wQBO conditions and none of them experienced a major midwinter SSW; by contrast the strong, easterly-QBO winter of 2023/24 produced two major SSWs (Table 1; Lee 2025). But n=3 is not sufficient to turn that correspondence into a causal explanation or a forecasting rule. The most defensible status is a hypothesis-generating observational pattern that can be tested against new events.

The claim of QBO-phase robustness must also be qualified at the level of definition. The three-of-three wQBO pattern is preserved under the 50-hPa November, 50-hPa November–December, 50-hPa DJF and 30-hPa November classifications, whereas under the 30-hPa DJF classification 1997/98 shifts to the easterly phase (Table A3). Particularly given that the 50-hPa DJF window overlaps the outcome period, a general statement of the form “robust under all QBO definitions” is not appropriate. The November 50-hPa wind is westerly but weak in the three super winters (+0.4, +1.2, +1.3 m s^{-1}), while the 30-hPa November values are more clearly westerly (+9.5, +5.7, +12.8 m s^{-1}). In randomizations that preserve the actual 30-hPa phase sequence, the reference probability that all three fall in the westerly phase is 0.091 under circular shifting and 0.056 under three-winter block permutation; although the approximate 0.06–0.09 range suggests that the pattern may not be entirely ordinary, it does not exclude a chance explanation given the small sample.

The fragility of the pattern is evident in the threshold sensitivity and in the counterexamples. In the strong-but-not-super band, 1957/58 (ONI +1.7) produced an SSW under wQBO, while 1991/92 (+1.5) passed without an SSW under eQBO. Although the November and DJF means were westerly in 2015/16, the disruption of the QBO in February 2016 (Osprey et al. 2016; Newman et al. 2016) further illustrates the physical limitation of a single-level classification. The wQBO phase therefore cannot be read as either a necessary or a sufficient condition for the absence of an SSW.

Changing the ruler affects the two components of the pattern in opposite directions. Under ONI≥+2.0 the cluster comprises three winters and is 3/3 wQBO and 3/3 SSW-free. When RONI≥+2.0 is used, 1991/92 joins the cluster: all four winters are SSW-free, but only three are wQBO (Table A2). In other words, the SSW-free component strengthens in the transition from ONI to RONI while QBO-phase purity weakens. The observational pattern that “super El Niño winters can be SSW-free” and the hypothesis that “this pattern is conditioned by wQBO” are therefore not equally index-robust. The first genuine eQBO super El Niño will be a case able to discriminate H2 more directly than the present 2026/27 configuration, whereas the expected wQBO of 2026/27 pushes the conditional expectations of H1 and H2 largely in the same direction.

A final nuance comes from the continuous measure behind the binary “SSW-free” label: vortex strength itself (Table 1, U10–60N column) shows that the three super winters are not homogeneous. The winter of 2015/16 carries one of the strongest vortices in the record (44.4 m s^{-1}; ~97th percentile), 1982/83 is above average (36.6 m s^{-1}; ~76th) and 1997/98 is below average (19.6 m s^{-1}; ~21st percentile) — it produced no SSW, but neither did it carry a strong vortex. The observation that “the vortex does not break down in super winters” should therefore not be read as “the vortex is always strong”; the common denominator is the absence of a reversal, and the continuous measure is carried forward to section 8.3 as a richer test variable than the binary label.

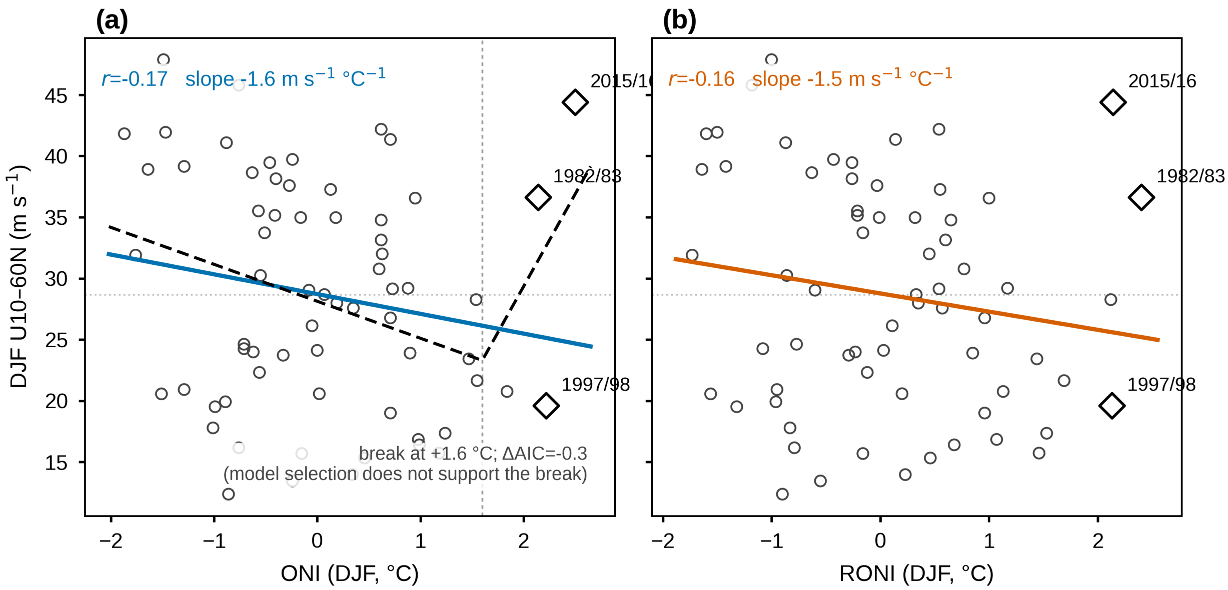

Figure 7. The continuous relationship between ENSO amplitude and polar vortex strength, winters 1959/60–2023/24 (*n*=66). (a) Scatter of ONI(DJF) against DJF U10–60N; the solid line is the linear fit and the dashed line the hinge model that allows a break at +1.6 °C. When the break point is counted as a free parameter, model selection does not support the break (ΔAIC=−0.3). (b) The same relationship using RONI. Diamonds mark the ONI≥+2.0 super winters. No simple relationship in which the vortex weakens systematically as El Niño amplitude increases is apparent, and the three super winters occupy very different vortex strengths (section 5). Data: NOAA CPC (ONI, RONI; ERSSTv6), NCEP/NCAR Reanalysis-1 (U10–60N; NOAA PSL); accessed 28 August 2026. Quantitative figure.

6. SSW Typology: A Subseasonal Descriptor

In an SSW the vortex is either pushed off the pole (displacement; predominantly wave-1) or separated into two cores (split; predominantly wave-2), and the view that this morphology differentiates the surface signature finds support in reanalysis composites: in split events Eurasian cooling is sharper and the downward response is about a week earlier (Nakagawa and Yamazaki 2006; Mitchell et al. 2013; Seviour et al. 2013; Hall et al. 2021). The opposing case is equally solid: Charlton and Polvani (2007), classifying with a zonal-mean criterion, find no meaningful difference; large model ensembles dissolve the difference beyond the first weeks (Maycock and Hitchcock 2015; White et al. 2019); and Lehtonen and Karpechko (2016) conclude that type information may not be a useful predictor for the surface. White et al. (2021) reconcile the two positions on the time axis: splits descend immediately and displacements with a lag of one to two weeks, while after three to four weeks the response becomes insensitive to morphology. The classification itself is method-dependent — the zonal-mean criterion and the moment-based diagnostic can assign different types in borderline cases (Charlton and Polvani 2007; Mitchell et al. 2013; Baldwin et al. 2021) — and the catalog does not provide a sample capable of testing the ENSO–type link (Barriopedro and Calvo 2014) (Table 1). Accordingly, SSW type is best treated as a subseasonal descriptor on the 0–2-week scale rather than as a seasonal predictor, and from a Turkish perspective the operative question is not morphology but whether the event couples downward and reverses the NAO. A summary of the literature composites is given in Appendix B (Table B1) and a schematic of the morphologies in Figure 4.

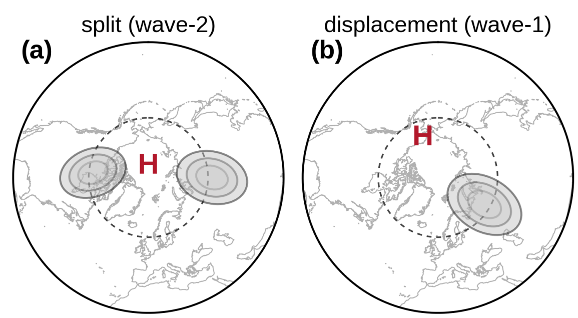

Figure 4. The two morphologies of major SSW events in north polar projection. (a) Split: the vortex separates into two cores, predominantly under wave-2 forcing. (b) Displacement: the vortex is pushed off the pole, predominantly under wave-1 forcing. H marks the center of the height anomaly. The method dependence of the classification and the discussion of the surface signature are given in section 6. This is a conceptual schematic: it is not a composite map produced from numerical fields and cannot be used for quantitative interpretation (section 2.3).

7. European–Turkish Teleconnections: The Anatomy of an Indirect Chain

The most direct quantitative link between the vortex state and Mediterranean precipitation is Zhang et al. (2024): in weak-vortex composites the Atlantic jet shifts southward, and total and extreme precipitation increase over the northern Mediterranean landmass while decreasing north of 45°N; the moisture budget shows that the dominant contribution comes from changes in vertical motion. The model experiment in the same study also marks the limit of the chain: WACCM reproduces the wave train descending from Greenland to Europe (stratospherically sourced) but not the train in the bottom-up tropospheric branch — the observed dipole cannot be attributed entirely to the stratosphere.

At the Turkish end the chain closes through the NAO/AO: the negative relationship between winter precipitation and the NAO is well documented at the national scale (Türkeş and Erlat 2003), and the link between the AO and mean winter temperatures has also been demonstrated (Türkeş and Erlat 2008). The most direct source for regional coefficients is Baltacı, Akkoyunlu and Tayanç (2018), who match 94 stations to five teleconnection patterns over 1965–2014: they report $r \approx -0.5$ for western Anatolian precipitation in the negative AO phase and −0.6 and −0.7 for Black Sea and Aegean warm-day frequencies, respectively, and identify the Genoa cyclone, which deepens in the negative phase, as the carrier mechanism; for the link between eastward-migrating Cyprus lows and the AO/North Sea–Caspian pattern, Sezen and Partal (2019) can be used. The eastern Mediterranean's own regulator, the EA/WR pattern, should be added to this picture: its positive phase dries the western Mediterranean while watering the eastern basin (Krichak et al. 2002; Trigo et al. 2006). At the event scale, the most direct Turkish case available to us is Kömüşcü and Oğuz (2021): in the winter of 2018/19 the combination of a vortex disruption with an omega block produced extreme cold and snowfall over Türkiye through cut-off lows that crossed the eastern Mediterranean and settled over the Marmara region.

Beyond these, no peer-reviewed study directly linking SSW type or QBO phase to Turkish precipitation and temperature at the station scale was identified among the sources we searched. This is not evidence of absence; the search does not rest on a systematic protocol (section 2.2). The regional inference in the present paper therefore has two layers: the vortex–Türkiye coefficients measured directly at the reanalysis scale in section 7.1, and the mechanism chain vortex → downward coupling → NAO/AO → Mediterranean storm track → Genoa/Cyprus cyclogenesis → Turkish surface climate. Every link of the chain can attenuate or reshape the signal, and the modest effect sizes of section 7.1 can be read as the quantitative counterpart of that dilution. For Türkiye, the value of seasonal monitoring therefore lies less in El Niño amplitude itself than in vortex evolution, downward coupling, the intraseasonal course of the NAO/AO and Mediterranean circulation.

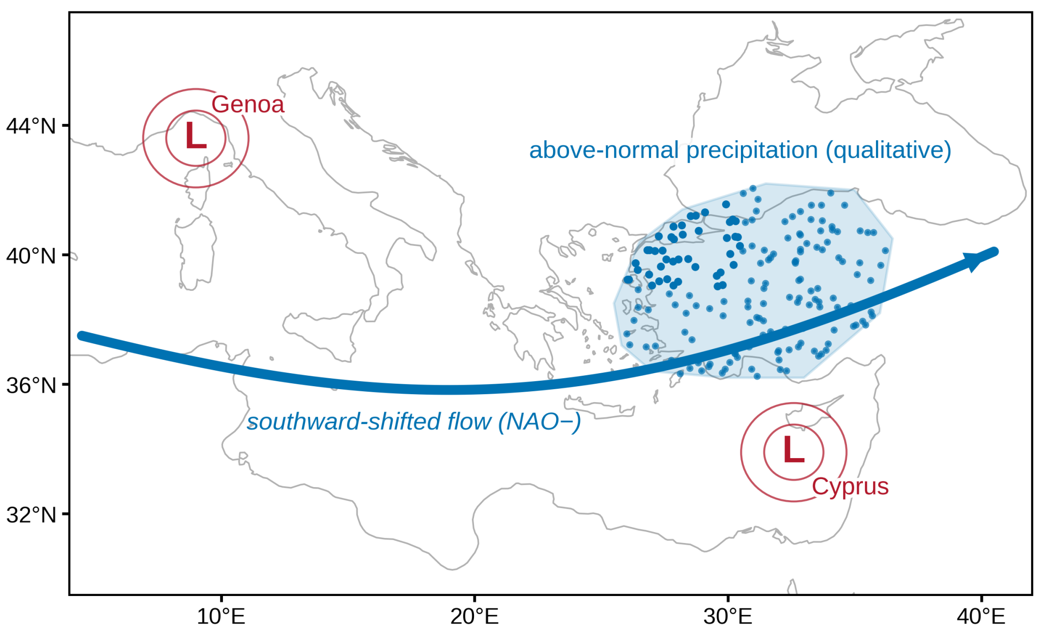

Figure 5. The Mediterranean storm track and the eastern Mediterranean/Türkiye precipitation window under a negative NAO regime. The southward-shifted flow, the Genoa and Cyprus cyclogenesis centers and the above-normal precipitation tendency concentrated around the Marmara–Aegean region are shown qualitatively. The quantitative counterpart of this end of the chain, measured with ERA5, is given in section 7.1 and Figure 9. This is a conceptual schematic: it is not a composite map produced from numerical fields and cannot be used for quantitative interpretation (section 2.3).

7.1 A direct observational test of the vortex–Türkiye link (ERA5)

The terminal link of the indirect chain is measured directly for the first time in this revision: for the winters 1979/80–2021/22 (n=43) the standardized DJF U10–60N was regressed on the monthly ERA5 Z500, precipitation and 2-m temperature fields, uncertainties were obtained from a winter-based bootstrap, and multiple comparisons over the grid domain were handled with BH-FDR (section 2.2). In the circulation layer the result is clear and consistent with expectations from the literature: a +1 standard deviation stronger vortex is associated with a positive-NAM-like pattern in DJF Z500 — a lowering of up to −28 m around Iceland and a rise of up to +8 m over the Azores ridge and +15 m over central Europe, with a sign close to zero over the eastern Mediterranean (Figure 9a). The coefficient reaches the local $p<0.05$ level at 42.0% of grid cells, and 36.6% pass the BH-FDR (α=0.10) criterion. JFM preserves the same structure with slightly weaker amplitude (Icelandic center −25 m; local 34.6%, FDR 25.4%), whereas in ND the pattern is both weak and mixed (18.8%/16.6%) and should be read with caution because of the partial acausality of the DJF predictor with respect to the ND response (section 2.2). The concurrent correlation of vortex strength with the NAO follows the same calendar: r=+0.41 in DJF, +0.45 in JFM and +0.10 in ND. In winters with a strong vortex the large-scale Atlantic–European circulation leans toward the side that relatively suppresses the southerly storm track carrying precipitation into the Mediterranean; in the weak-vortex reading the signs reverse symmetrically.

In the precipitation layer the signal is measurable but modest and spatially heterogeneous: the fraction of grid cells passing FDR is 1.5% in DJF, 0% in ND and 1% in JFM, and none of the fifteen regional coefficients passes the family-level BH-FDR (α=0.10) threshold (section 2.2), so the individual intervals below should be read as exploratory. In the regional means, however, DJF gives a consistent dry-signed tendency: a +1 standard deviation stronger vortex corresponds to −5.49 mm month^{-1} for the Türkiye box (−6.8% of the climatology; 95% CI −10.47/−0.83; p=0.022), −9.69 for the Aegean (−10.0%; −17.81/−1.60) and −5.46 for Marmara (−6.9%; −10.90/−0.22), while the intervals for the Mediterranean coast (−8.79; −19.29/+1.53) and the Levant (−2.79; −8.62/+3.08) include zero (Figure 9b, d). In the ND window the signal shifts southward: the Mediterranean coast (−11.89; −12.1%; −24.72/−0.55) and the Levant (−6.55; −11.1%; −12.89/−0.37) exclude zero while the Türkiye box becomes indeterminate (−4.28; −10.91/+2.30). In JFM the intervals include zero in all five regions (Türkiye box −2.25; −6.67/+1.72): the prior expectation derivable from the two-pathway literature that the late-winter link is stronger is not confirmed for precipitation, and JFM turns out to be the weakest of the three windows. There is no contradiction between individual intervals that exclude zero and the family-level threshold not being passed: a signal visible when one region is examined on its own is not strong enough to exceed the multiple-comparison threshold when all fifteen regional tests are evaluated together. These coefficients therefore represent not a deterministic rule for Turkish precipitation but a probability shift that is consistent in sign yet statistically fragile. For weak-vortex winters the sign of all these coefficients reverses: −1 standard deviation implies a wet-signed tendency of order +5.5 mm month^{-1} for the Türkiye box in DJF.

The role of the NAO differs by window. In DJF, controlling for the NAO barely changes the Türkiye coefficient (Model A −5.49 → Model B −5.28) and the bootstrap interval of the indirect component includes zero (−0.14; −2.34/+1.82): the midwinter link appears to carry a component that cannot be reduced to the monthly NAO index. In JFM the picture is reversed: adding the NAO erases the Türkiye coefficient (−2.25 → +0.10) and the indirect component excludes zero (−2.18; −5.46/−0.14; for Marmara −4.11; −8.56/−0.73). The U10 coefficient is thus substantially attenuated in late winter once the NAO is included, which is consistent with variance shared with the NAO but does not demonstrate a one-way causal mediation. This is an observational Model A/B decomposition, not a causal path analysis (section 2.2); nonetheless, the fact that it coincides with the “descent through the NAO” expectation of downward coupling in late winter but not in midwinter is a distinction worth noting for the discussion of mechanisms. In late winter a substantial part of the vortex–Turkish precipitation relationship appears to travel in the same information channel as the component of the Atlantic–European circulation measured by the NAO. This pattern is compatible with an interpretation in which the connection is an indirect pathway carried by the NAO; it is not proof of mediation.

The temperature layer is secondary: although 17.9% of grid cells are locally significant in the DJF T2m pattern, only 2.0% pass the FDR criterion, and the Türkiye regional coefficients are indeterminate in all windows (DJF −0.22 K, 95% CI −0.57/+0.11; JFM −0.23; −0.63/+0.17). Taken together, a strong vortex is associated, through a +NAM circulation pattern in which more than a third of the grid cells pass FDR, with a dry-signed probability shift over Türkiye in midwinter of order 7–10% of climatology, and with a symmetric wet-signed shift under a weak vortex; the signal moves to the southern coastal belt in November–December and disappears at the regional scale in January–March. The full coefficient table and the ND/JFM maps are given in Appendix C; the place of these results in the 2026/27 monitoring framework is discussed in section 8.3 and their limitations in section 9.

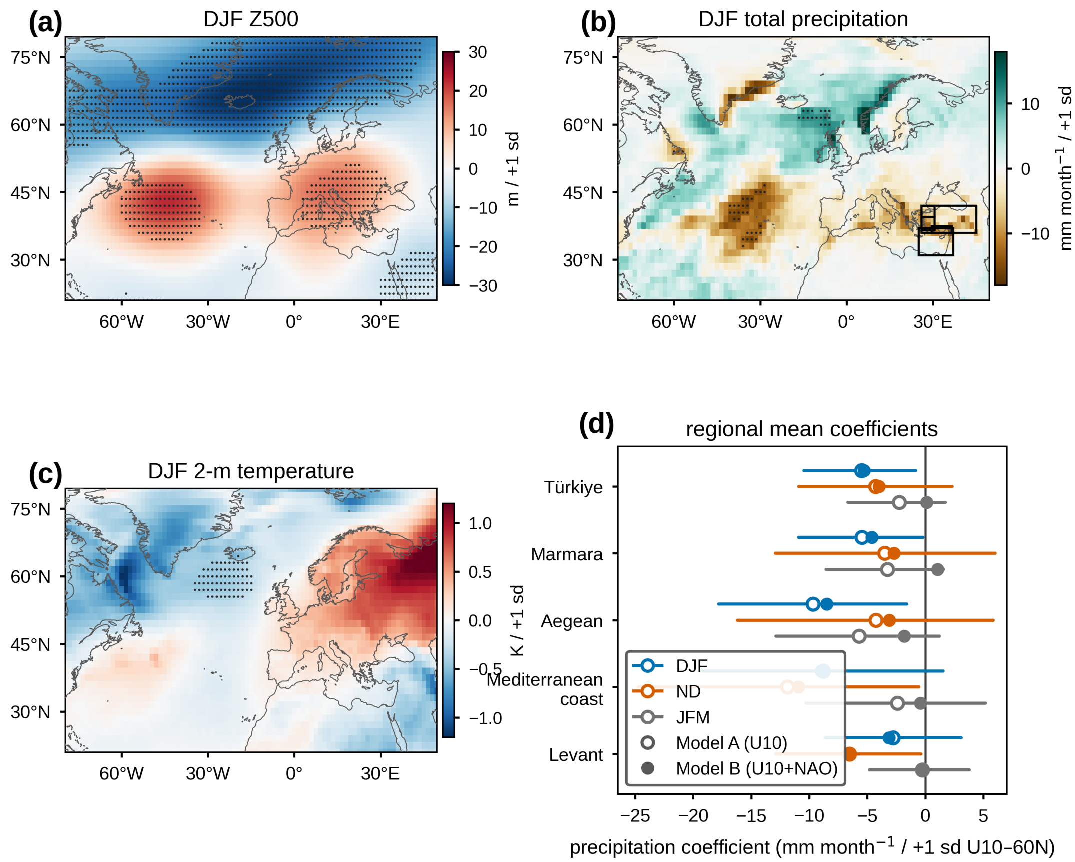

Figure 9. The concurrent regional signature of vortex strength in ERA5: regression on standardized DJF U10–60N, winters 1979/80–2021/22 (n=43; anomalies relative to the 1991–2020 climatology). (a) DJF Z500 coefficient (m per +1 sd); stippling marks grid cells whose winter-based bootstrap 95% interval excludes zero and which pass the BH-FDR (α=0.10) criterion. (b) DJF precipitation coefficient (mm month^{-1} per +1 sd) and the five a priori regional boxes. (c) DJF 2-m temperature coefficient (K per +1 sd). (d) Regional mean precipitation coefficients and their 95% bootstrap intervals; open symbols denote Model A (U10 only) and filled symbols Model B (U10 + NAO); colors denote the DJF/ND/JFM windows. The figure shows the vortex → 500-hPa circulation → Turkish precipitation/temperature links in a single frame; the circulation pattern in (a) passes the BH-FDR criterion at 36.6% of grid cells, whereas the corresponding fraction for the precipitation pattern in (b) is 1.5% — the circulation link is markedly more robust than the precipitation link. The regional boxes are cosine-latitude-weighted full-area means; no land–sea mask is applied. Signs reverse for weak-vortex winters. Data: ERA5 (WeatherBench2 1.5° monthly derivative; Hersbach et al. 2020; Rasp et al. 2024), NCEP/NCAR R1 (U10), CPC (NAO); accessed 29 August 2026. Quantitative figure.

8. Winter 2026/27: A Prospectively Defined Conditional Observational Update

8.1 Initial conditions (August 2026)

As of late August 2026, Niño-3.4 stands at +2.7 °C weekly and +2.03 °C for the July monthly mean; CPC keeps the probability of the “very strong” category above 90% and the October–December RONI median at +2.66 °C (interquartile range +2.37/+2.95), and assigns a 69% probability to a historic peak exceeding all events since 1950; ECMWF members place the Niño-3.4 peak in the +3.5–4.5 °C band; in the IRI plume, 25 of 26 models fall in the “very strong” category for October–December while 15 models give +3.0 °C or more; and MEI.v2 reaches +2.41 for June–July 2026, the highest June–July value in the post-1979 record. This unusual amplitude offers a strong opportunity to update the conditional expectations of sections 3 and 5 with a new extreme observation; it is not by itself a mechanism-separating experiment. On the QBO side the westerly regime is descending from above — the westerly front was at 40 hPa in July (+9.0 m s^{-1}; 30 hPa +14.3) and the 50-hPa easterly has weakened to −6.5 m s^{-1} — and a simple descent extrapolation predicts that 50 hPa will turn westerly in November–December; if that phase materializes, the expectations of H1 and H2 will point largely in the same direction. The vortex itself is on its climatological schedule: mid-August analyses find no evidence of early formation. Table 4 places these initial conditions alongside the historical analogs.

Table 4. Super El Niño winters and 2026/27. ONI: NOAA CPC, ERSSTv6, `oni.ascii.txt`, accessed 28 Aug 2026. QBO50(Nov): sign of the CPC/CDAS 50-hPa November mean. The NAO column runs November–December → January–March.

Winter	**ONI (DJF)**	QBO50 (Nov)	Major SSW	NAO (ND→JFM)	Note
1982/83	+2.1	W	None	+1.69 → +0.67	The RONI record (+2.40) belongs to this event
1997/98	+2.2	W	None	−0.93 → +0.38	Exception to the composite: entered the winter with a negative NAO
2015/16	+2.5	W	None	+1.99 → +0.81	February 2016 QBO disruption; record-strength vortex
2023/24	+1.8	E	16 Jan [D]; 4 Mar [S]	+0.81 → +0.36	Sub-super analog; two events under easterly QBO
2026/27	to be monitored (forecast ≥ +2.0)	W (descending; to be monitored)	to be monitored	to be monitored	RONI OND median +2.66; QBO disruption is the wild card

8.2 Competing explanations

Three explanations are on the table for the SSW-free super winters of the record, but 2026/27 cannot deliver a single-winter verdict among them. If the expected wQBO materializes, H1 and H2 generate expectations in the same direction — less favorable conditions for an SSW and a relatively stronger vortex — so the winter will not separate the two cleanly. The more discriminating natural case would be a genuine super El Niño occurring under eQBO conditions. The function of 2026/27 is narrower and more defensible: to show to what extent conditional expectations defined before the outcome was known gain or lose support against SSW occurrence and the continuous evolution of U10–60N. The H1–H3 framework below should therefore be read as a sequential observational evidence update rather than as a confirmation/falsification scheme.

H1 — Saturation/nonlinearity. The physical hypothesis proposes that, as ENSO amplitude increases, the effective planetary-wave forcing transmitted to the stratosphere by tropical convection and the Aleutian Low response may not grow proportionally; one candidate mechanism is a loss of efficiency at the amplitude end in the constructive interference of the ENSO-driven wave pattern with climatological wave-1 (Zhou et al. 2019). The present study does not measure that mechanism directly. The relationship between ONI/RONI and DJF U10–60N and the segmented fit test only the continuous signature expected at the downstream vortex level under a simple saturation scenario; $r=-0.17$ and ΔAIC$=-0.3$ provide no support for that signature. If U10–60N in 2026/27 remains close to the historical super-winter range despite record ENSO amplitude, that would be compatible with H1 but would not by itself count as mechanistic evidence, whereas a markedly weak vortex or a major SSW would reduce the relative weight given to a simple plateau expectation. A more direct test of H1 should examine how wave-driven meridional heat transport (eddy heat flux, $v'T'$) at 100 hPa in the 45–75°N band — the standard indicator of upward wave activity — together with the EP flux, the wave-1 amplitude and, if possible, a metric of constructive interference between the ENSO-driven anomaly and climatological wave-1, varies with amplitude.

H2 — QBO modulation. The Holton–Tan framework requires the QBO to be viewed not as a deterministic switch but as a background condition that probabilistically alters the sensitivity of the polar vortex to planetary-wave forcing. In our own data, under the main November 50-hPa definition the eQBO/wQBO SSW risk is 12/19 versus 13/26 (RR=1.26; 95% CI 0.75–2.12), and in the long 30-hPa record RR=1.48 (0.94–2.32). Although the direction is largely consistent, the intervals include unity and the ENSO×QBO interaction cannot be resolved. A major SSW under wQBO in 2026/27 would therefore not falsify H2; it would only break the present n=3 "super El Niño + wQBO + no SSW" pattern and reduce the relative weight given to the QBO explanation. Conversely, the absence of an SSW under wQBO would not confirm H2 and would not separate H1 from H2. If the phase remains easterly, or if the pre-winter profile turns easterly, the case becomes more discriminating with respect to H2; even then, a single winter is an information update rather than a verdict on a probabilistic hypothesis.

H3 — Ordinary/internal variability. This explanation holds that blocking sequences and the internal atmospheric timing of wave packets play a large role in SSW occurrence, and that the clustering across three super winters may not require a special mechanism. In randomizations preserving the actual QBO sequence, the reference band of about 0.06–0.09 for a 3/3 wQBO match suggests that the pattern may not be entirely ordinary, but with n=3 this is not sufficient to exclude a chance explanation. The counterexamples of 1957/58 (wQBO with an SSW) and 1991/92 (eQBO without an SSW) also keep H3 on the table. A wQBO and SSW-free outcome in 2026/27 would extend the pattern and could place additional pressure on H3, whereas wQBO with an SSW would weaken it. Neither outcome is by itself sufficient to accept or reject internal variability.

8.3 Prospectively defined discriminating observations and evidence updating

The following outcomes will be interpreted with the same criteria, fixed before the winter occurs. (i) If the November

50-hPa mean remains easterly, or if a persistent easterly layer appears in the 40–50-hPa descent profile, 2026/27 becomes more discriminating with respect to H2; the cleanest natural separation remains a genuine super El Niño under eQBO. (ii) If wQBO materializes and a major midwinter SSW occurs, H2 is not thereby falsified on its own; the present 3/3 pattern breaks, the relative weight given to QBO conditioning decreases, and the simple saturation/plateau expectation also weakens. (iii) The absence of an SSW under wQBO together with a strong U10–60N would extend the pattern by one event and could place additional pressure on H3, but it would not separate H1 from H2 and would confirm neither. (iv) If U10–60N remains close to the historical super-winter distribution despite record ENSO amplitude, that will be counted as compatible with the vortex-level expectation of the simple saturation scenario, whereas a marked weakening will be counted as less compatible with it. This comparison will use the continuous measure alongside the binary SSW label, but because planetary-wave forcing is not measured directly it will not be converted into a mechanistic verdict on H1. The differences between the RONI and ONI rulers and the counterexamples of 1991/92 and 2023/24 will be retained as the sensitivity limits of the interpretation.

From an eastern Mediterranean perspective the inference is now quantified but still cautious. This study produces direct coefficients at the reanalysis scale between U10–60N and Türkiye box-mean precipitation (section 7.1): in DJF a +1 standard deviation stronger vortex means −5.5 mm month^{-1} for the Türkiye box, and a weak vortex a symmetric wet-signed tendency — of order 7% of climatology, probabilistic rather than deterministic. A station-scale coefficient has still not been produced, and every link of the chain vortex → downward coupling → NAO/AO → Mediterranean storm track → Türkiye can dilute the signal. For that reason the 2026/27 monitoring set should follow, more closely than El Niño amplitude itself, the late-November QBO profile, jumps in wave-driven heat transport at 100 hPa in the 45–75°N band, the 10-hPa 60°N wind, the downward NAM/AO signal, the intraseasonal direction of the NAO and Mediterranean circulation together. The early-winter r=+0.21 and late-winter r=−0.12 values are not a deterministic precipitation calendar for Türkiye; they show only why intraseasonal teleconnection differentiation must be taken into account in regional interpretation.

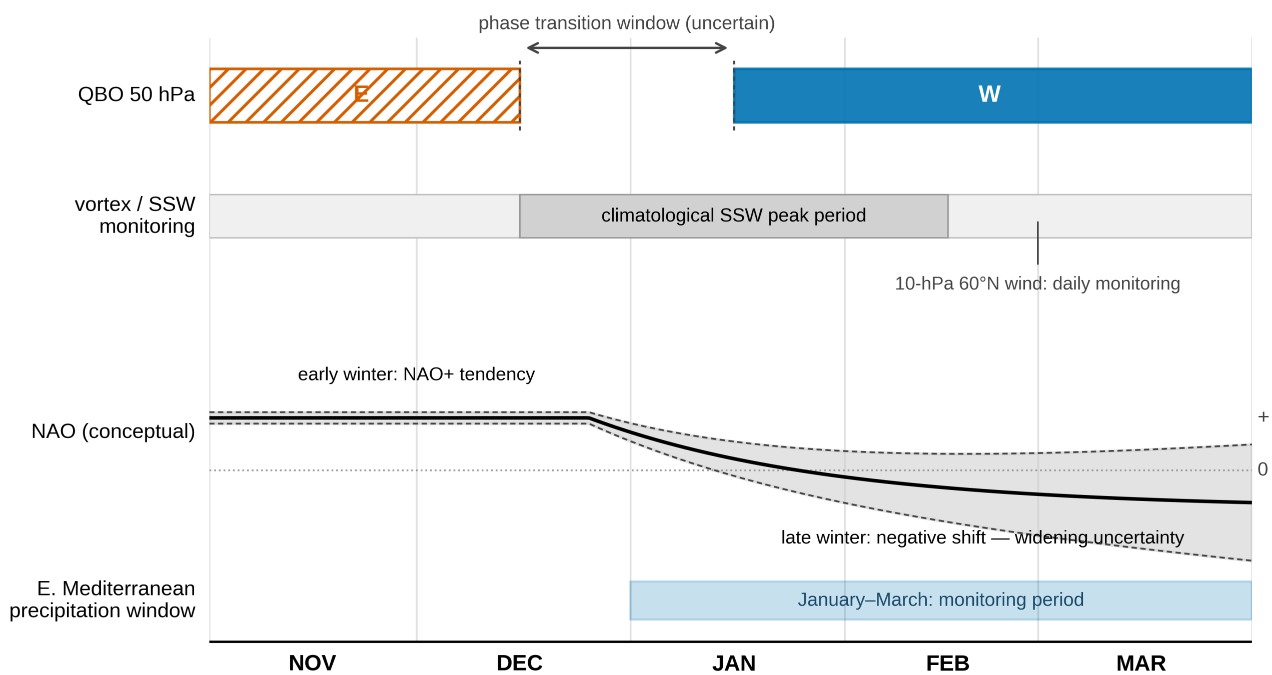

Figure 6. Monitoring calendar for the winter of 2026/27. The rows show, in order, the expected evolution of the 50-hPa QBO phase and the uncertainty of the phase transition window; the vortex/SSW monitoring period together with the climatological peak range of SSWs; the conceptual evolution of the NAO with a widening uncertainty fan; and the eastern Mediterranean precipitation window. The calendar is not a forecast but the order in which the discriminating observations defined in section 8.3 will be monitored. This is a conceptual schematic: it is not a composite map produced from numerical fields and cannot be used for quantitative interpretation (section 2.3).

9. Discussion

The ENSO–NAO result should be read through the difference between the two intraseasonal windows rather than through the strength of the individual correlations. In early winter r=+0.21 and in late winter r=−0.12, and both individual confidence intervals include zero; by contrast the paired difference is Δr=+0.33 (95% CI +0.08/+0.56) and remains away from zero under the moving block bootstrap. This does not show that ENSO deterministically causes a positive NAO in early winter and a negative NAO in late winter. The more defensible conclusion is that the ENSO–NAO relationship can differentiate systematically within the same winters and that a single DJF mean (r=−0.04) can mask that structure by adding opposing tendencies. The facts that late-winter behavior in the composites is more often a weakening than a full sign reversal, and that exceptions such as 2015/16 exist, preserve that limit.

For the QBO the seasonal-mean surface correlation is close to zero (QBO50×AO r=−0.01), whereas the winter-based probability of a major SSW appears higher under eQBO. Under the main November 50-hPa definition RR=1.26 (95% CI 0.75–2.12) and in the long 30-hPa record RR=1.48 (0.94–2.32); the value of 1.71 obtained with the DJF definition, which overlaps the outcome period, is an upper bound. That the confidence intervals include unity shows that the magnitude of the effect cannot be pinned down with the present record. The QBO is therefore not a switch but a conditioner whose direction is largely consistent across the main definitions while the magnitude of the probability shift remains uncertain. The ENSO×QBO interaction cannot be resolved because of both the small cell counts and the sensitivity to definition; the present data neither demonstrate nor exclude an interaction.

The two components of the super El Niño pattern do not carry the same epistemic weight. That 1982/83, 1997/98 and 2015/16 are 3/3 wQBO and 3/3 SSW-free under ONI≥+2.0 is notable, but n=3 keeps this at the level of a hypothesis-generating pattern. The QBO-phase result is preserved under the 50-hPa November, November–December and DJF definitions and under 30-hPa November, while 1997/98 changes phase under 30-hPa DJF; the statement "robust under all QBO definitions" should therefore not be used. The sequence-preserving permutation reference of 0.06–0.09 does not exclude chance. More importantly, the RONI≥+2.0 ruler adds 1991/92 and raises the SSW-free component to 4/4 while lowering wQBO purity to 3/4. The "super El Niño–no SSW" pattern thus strengthens under the change of index while the hypothesis that this is explained by wQBO weakens. Under the expected wQBO, 2026/27 will not separate these two explanations cleanly; the more discriminating future case is an eQBO super El Niño.

In the saturation debate, U10–60N measures only the downstream vortex response. The ONI–U10 relationship is r=−0.17 (p=0.16) and the segmented fit gives ΔAIC=−0.3, so the vortex-level continuous signature of the simple "weakens with amplitude, then plateaus" scenario is not supported in the present observational record. This result is not a direct rejection of the planetary-wave forcing mechanism. A more direct test of H1 should examine wave-driven meridional heat transport ($v'T'$) at 100 hPa in the 45–75°N band, the EP flux and the planetary wave-1 amplitude and, if possible, the constructive interference of the ENSO-driven anomaly with climatological wave-1 across amplitude. In the continuous regression, adding wQBO raises R^2 from 0.002 to 0.126 and the coefficient is +6.79 m s^{-1} (95% CI +1.19/+12.39); this measurable relationship is of interest, but it was produced from NCEP/NCAR Reanalysis-1 alone. The coefficient magnitude, the super-winter percentiles and the ONI/RONI–U10 results should not be described as "reanalysis-independent" or "robust across reanalyses" until they have been retested with ERA5 and, if possible, JRA-55. A first step at the predictor level was taken in this revision: the NCEP R1 U10 series was independently rederived and matched the catalog exactly, with the R1–R2 comparison giving r=0.9997, a mean difference of +0.15 m s^{-1} and an RMS difference of 0.28 m s^{-1}; deriving 10 hPa from ERA5 remains a prospectively defined item of future work because of the monthly access restriction for anonymous users.

The limitations combine at the level of sample, data product and regional inference. The ENSO×QBO cells are small; the SSW catalog does not extend before 1958 and the 50-hPa QBO series does not extend before 1979; the SSW split/displacement classification is method-dependent, and the surface impact is not fully agreed upon in model and reanalysis studies, particularly at the seasonal scale. At the regional end this revision has taken a step: the core of the design proposed as future analysis in the second round — pairing the vortex metric with ERA5 fields in a multivariate framework that also accounts for the NAO/AO — was implemented in section 7.1 and, for the first time, converted the link between vortex strength and Türkiye box-mean precipitation into coefficients with confidence intervals. The parts not implemented are recorded with equal clarity: the analysis is at the reanalysis grid scale, not at the station scale; it is built on concurrent seasonal windows, so 0–60-day lagged and distributed-lag designs and event-based composites still lie in the future; the NAO "mediation" is an observational Model A/B comparison, not a causal path analysis; the setup of the ND window with the DJF predictor is partly acausal (the pattern correlation with the concurrent predictor falls to 0.68); at 1.5° resolution the regional boxes are coarse; in all five boxes the average is a cosine-latitude-weighted full-area mean that also includes ocean cells; and coastal representation is limited at this resolution. No coefficient in the family of fifteen regional coefficients passes the BH-FDR (α=0.10) threshold, and individual intervals that exclude zero are exploratory. The findings of section 7.1 also discipline the interpretation: the prior expectation that the late-winter link is stronger was not confirmed for precipitation, and JFM turned out to be the weakest of the three windows; by contrast, controlling for the NAO erases the coefficient only in JFM. This distinction — that the midwinter link carries a component that cannot be reduced to the monthly NAO index while the late-winter coefficient is erased once the NAO is added — coincides in late winter with the "descent through the NAO" expectation of the downward coupling literature and is left as an observation capable of separating mechanism hypotheses.

10. Conclusions

The findings can be summarized under five headings; in each, the observational result is separated from the stronger claim that cannot be drawn from it.

1) Intraseasonal structure of ENSO–NAO. The ONI–NAO correlation is r=+0.21 in early winter and r=−0.12 in late winter; both individual relationships are weak and their confidence intervals include zero. By contrast, the paired difference over the same winters is Δr=+0.33 (95% CI +0.08/+0.56) and is preserved under the moving block bootstrap. What is strong is therefore not the individual correlations but the differentiation between early and late winter. This finding does not show that ENSO causes a particular NAO sign; it shows that a single DJF mean (r=−0.04) can hide opposing intraseasonal tendencies. Its physical counterpart is consistent with the relative prominence of the tropospheric pathway in early winter and of the pathway descending through the stratosphere in late winter; its limit is that the individual relationships remain weak.

2) QBO / Holton–Tan. The QBO50×AO seasonal-mean correlation is close to zero (r≈−0.01). For winter-based major SSW risk, the main November 50-hPa definition gives RR=1.26 (95% CI 0.75–2.12) and the long 30-hPa record RR=1.48 (0.94–2.32); the RR=1.71 obtained with the DJF definition, which overlaps the outcome period, should be read as an upper bound. Because the intervals include unity, the effect size is not precise. Westerly QBO does not prevent sudden stratospheric warmings; in the present record it only shifts the probability weight. The QBO here is not a forcing that shifts surface indices deterministically but a conditioner able to change event probabilities by a limited and uncertain amount, and the ENSO×QBO interaction cannot be resolved with the present data. For that reason a single SSW under wQBO in 2026/27 will not falsify H2, and the absence of an SSW will not confirm it.

3) The super El Niño pattern. That 1982/83, 1997/98 and 2015/16 are 3/3 wQBO and 3/3 SSW-free under ONI≥+2.0 is notable, but because n=3 it is a hypothesis-generating observational pattern rather than evidence. When RONI≥+2.0 is used, 1991/92 joins the cluster: the SSW-free component strengthens to 4/4 while wQBO purity falls to 3/4. The SSW-free component thus strengthens under the change of ruler while QBO-phase purity weakens, so the two propositions are not equally index-robust. The 3/3 wQBO pattern is preserved under the 50-hPa November, November–December and DJF definitions and under 30-hPa November, but 1997/98 changes phase under 30-hPa DJF. The sequence-preserving permutation reference of 0.06–0.09 does not exclude a chance explanation. The more discriminating future observation is a genuine super El Niño under eQBO conditions.

4) Saturation and the continuous vortex. The ONI–U10–60N relationship is weak and consistent with zero (r=−0.17; p=0.16), and the segmented model does not outperform the linear one (ΔAIC=−0.3). The U10 values of the super trio are not homogeneous. The vortex-level continuous signature expected under a simple saturation scenario is therefore not supported in the observational record; but the analysis is not a direct test of planetary-wave forcing, since U10–60N measures not the forcing the waves apply to the vortex but the final response of the vortex to that forcing. In the joint sample the ONI-only model gives R^2=0.002, while adding wQBO raises R^2 to 0.126 with a wQBO coefficient of +6.79 m s^{-1} (95% CI +1.19/+12.39; p=0.019); the additional explanatory power of the ENSO×QBO term is very small. Because this regression rests on NCEP/NCAR Reanalysis-1, the coefficient and the super-winter percentiles should be retested with ERA5 and, if possible, JRA-55; product-independent robustness has not yet been demonstrated.

5) 2026/27 and the eastern Mediterranean. No direct “El Niño amplitude → precipitation/temperature” rule can be derived for Türkiye; by contrast, the vortex strength → Turkish precipitation link was tested directly in this revision and a quantitative bridge for the stratosphere–Türkiye chain was established for the first time — a bridge built with a single reanalysis product, over a single period and without station verification. In DJF a +1 standard deviation of vortex strength is associated with a positive-NAM Z500 pattern in which 36.6% of grid cells over the Atlantic–European sector pass the BH-FDR (α=0.10) criterion, and with a precipitation anomaly of −5.5 mm $month^{-1}$ [95% CI −10.5/−0.8] in the Türkiye box (Aegean −9.7, Marmara −5.5; in November–December the signal shifts to the Mediterranean coast at −11.9 and the Levant at −6.6); the signs reverse in weak-vortex winters. The effect sizes are of order 7–12% of the regional climatologies, the fraction of grid cells passing FDR for precipitation is low, none of the fifteen regional coefficients passes the family-level BH-FDR threshold, and the regional signals disappear in January–March: this link is a probabilistic tendency, not a deterministic rule. The strength of the evidence is not equal across layers: the 500-hPa circulation link passes the multiple-comparison threshold at more than a third of grid cells, whereas the Turkish precipitation signal is consistent in sign but statistically fragile. The physical chain to be monitored is QBO → planetary-wave forcing → polar vortex → downward stratosphere–troposphere coupling → NAO/AO → Mediterranean storm track → Türkiye, and section 7.1 has given a measured magnitude to the terminal link of that chain. Winter 2026/27 is a prospectively defined conditional observational update; a single winter will deliver no verdict on any hypothesis and will only update the relative observational weight given to them: wQBO with an SSW would break the present 3/3 pattern and could reduce the relative weight given to H2 but would not falsify it, whereas wQBO without an SSW could extend the pattern but would not separate H1 from H2. The next quantitative step toward reducing regional uncertainty is to test these coefficients at the station scale with Türkiye's long station series and with a 0–60-day lagged design.

This study shows that ENSO amplitude alone is insufficient to explain the state of the polar vortex, and that in the present record the QBO appears as a conditioner that is more evident than ENSO amplitude yet limited and probabilistic. The super El Niño–no SSW pattern is notable, but it remains at the status of a hypothesis because of the small sample; moreover, the SSW-free component is more resistant than QBO-phase purity to a change of the ONI/RONI ruler. The present saturation analysis is not a direct mechanistic test of planetary-wave forcing, and the continuous vortex result rests on a single reanalysis product; by contrast, the European–Mediterranean end of the chain has been measured independently with ERA5 and the regional effect sizes are given with confidence intervals (section 7.1). Winter 2026/27 is therefore not a decisive confirmation or falsification experiment but an observational test in which prospectively defined conditional expectations will be updated against a new extreme observation. Its scientific value lies not in extracting a winning hypothesis from a single winter but in showing, transparently and reproducibly, how the relative observational support given to saturation, QBO modulation and internal variability should be reweighted as new information arrives.

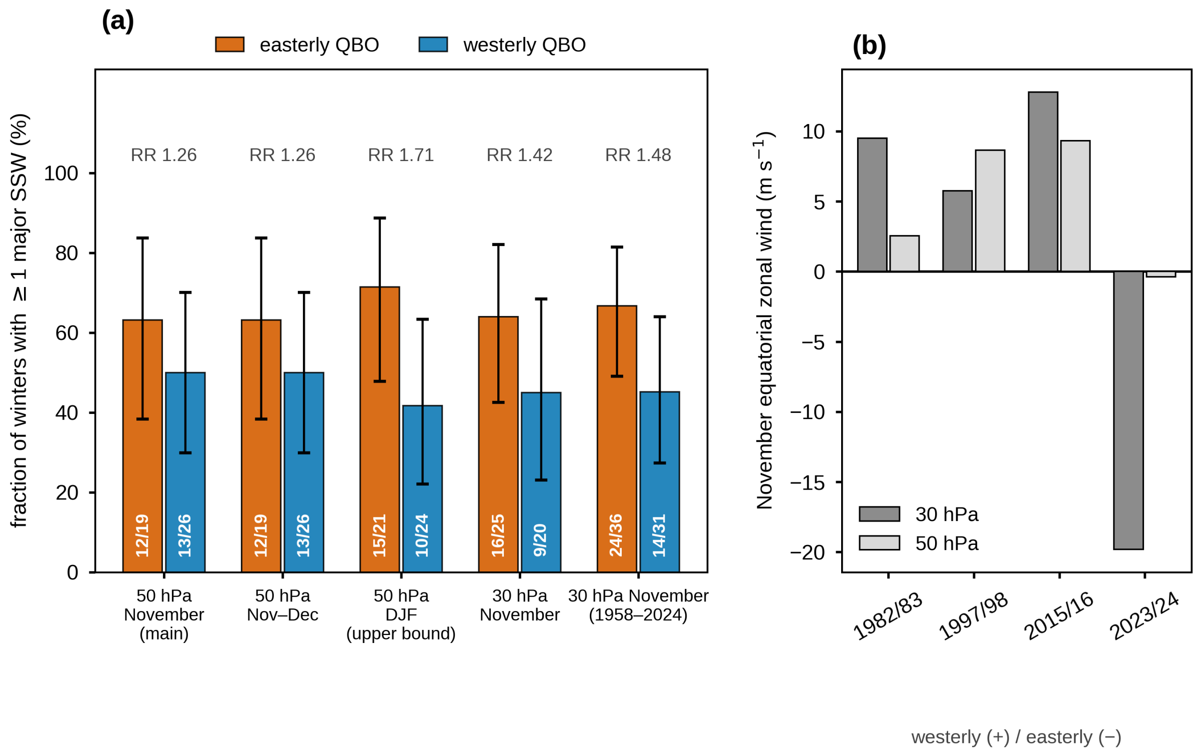

Figure 8. Under all five phase definitions the easterly-QBO side indicates a higher fraction: the direction is relatively consistent, the magnitude uncertain. (a) Sensitivity of the fraction of winters with at least one major SSW to the QBO phase definition; bars are Clopper–Pearson exact 95% intervals and the labels give the numerator and denominator counts. (b) The 30- and 50-hPa November equatorial zonal wind for the super winters and for 2023/24. Panel (b) shows the November classification only; under the 30-hPa DJF sensitivity definition 1997/98 moves to the easterly phase (Table A3), so phase robustness should not be generalized as holding under all definitions. Data: CPC/CDAS (50 hPa, 1979–), NOAA PSL (30 hPa, 1948–), NOAA CSL SSW Compendium; accessed 28 August 2026. Quantitative figure.

Tables

Table 1. Catalog of El Niño winters (ONI_DJF ≥ +0.5; 1951–2024). QBO50(Nov) and QBO30(Nov): sign of the November mean of the 50-hPa (CPC/CDAS, 1979–) and 30-hPa (NOAA PSL, 1948–) equatorial zonal-mean wind; the labels are derived independently of the SSW catalog. U10–60N: 10-hPa 60°N DJF zonal-mean wind, m s^{-1} (NCEP/NCAR R1; 1959–2024 climatology 28.7 ± 9.3 m s^{-1}). ONI: NOAA CPC, ERSSTv6. All series accessed 28 August 2026.

Winter	**ONI (DJF)**	QBO50 (Nov)	QBO30 (Nov)	U10–60N	SSW (ERA5 central date) [type†]	NAO (ND)	NAO (JFM)	**AO (DJF)**
1951/52	+0.5	—	E	+25.7	—	+0.47	−0.46	+0.20
1957/58	+1.7	—	W	+24.9	8 Feb 1958	+0.42	−1.19	−0.95
1958/59	+0.6	—	E	+30.8	Nov 1958 (absent in ERA5)	+0.47	−0.11	−0.39
1963/64	+0.9	—	W	+36.6	—	−1.59	−1.19	−0.46
1965/66	+1.2	—	E	+17.3	16 Dec 1965; 22 Feb 1966	−0.14	−0.86	−1.50
1968/69	+1.0	—	E	+16.8	28 Nov 1968; 13 Mar 1969	−1.17	−1.31	−2.29
1972/73	+1.6	—	E	+21.6	31 Jan 1973	+0.36	+0.40	+1.09
1976/77	+0.7	—	E	+19.0	9 Jan 1977	−0.72	−0.78	−2.62
1977/78	+0.7	—	E‡	+26.8	—	−0.54	−0.28	−1.20

Winter	**ONI (DJF)**	QBO50 (Nov)	QBO30 (Nov)	U10–60N	SSW (ERA5 central date) [type†]	NAO (ND)	NAO (JFM)	**AO (DJF)**
1979/80	+0.6	E	E	+34.8	29 Feb 1980	+0.77	−0.34	−0.57
1982/83	+2.1	W	W	+36.6	—	+1.69	+0.67	+0.17
1986/87	+1.2	W*	E	+15.7	23 Jan 1987	+1.64	−0.58	−0.85
1987/88	+0.6	W	W	+32.0	8 Dec 1987; 14 Mar 1988	+0.25	+0.54	−0.45
1991/92	+1.5	E	E	+28.3	—	+0.47	+0.60	+1.09
1994/95	+0.9	E	E	+29.2	—	+1.33	+1.11	+0.72
1997/98	+2.2	W	W	+19.6	—	−0.93	+0.38	−0.78
2002/03	+0.9	W	W	+23.9	18 Jan 2003	−0.56	+0.37	−0.65
2004/05	+0.6	W	W	+42.2	—	+0.97	−0.12	+0.11
2006/07	+0.6	W	W	+33.1	24 Feb 2007	+0.89	+0.40	+1.00
2009/10	+1.5	W*	E	+23.4	9 Feb 2010 [S]; 24 Mar 2010 [D]	−0.97	−1.32	−3.42
2014/15	+0.7	E	E	+29.1	—	+1.27	+1.52	+0.85
2015/16	+2.5	W	W	+44.4	—	+1.99	+0.81	−0.01
2018/19	+1.0	E*	W	+16.4	1 Jan 2019 [S]	+0.25	+0.70	+0.18
2019/20	+0.7	W	W	+41.4	—	+0.74	+1.20	+2.08
2023/24	+1.8	E	E	+20.8	16 Jan 2024 [D]; 4 Mar 2024 [S]	+0.81	+0.36	+0.07

ND = November–December; JFM = January–February–March. "—" = no CPC 50-hPa data before 1979; the phase for these winters is derived from 30 hPa only. ‡ = November value very close to zero (−0.3 m s^{-1}), so the classification is borderline. * = the November labels of the two levels disagree; across the full catalog the winters that disagree are 1983/84, 1986/87, 1988/89, 1992/93, 1993/94, 1995/96, 2009/10, 2011/12, 2017/18 and 2018/19. † The split (S) / displacement (D) classification is method-dependent (the zonal-mean criterion of Charlton and Polvani 2007 and the 2-D moment diagnostic of Mitchell et al. 2013 can diverge in borderline cases; see Baldwin et al. 2021); a type is assigned only to recent events for which there is broad agreement in the literature, and disputed cases are marked with an asterisk. The 2023/24 events postdate the compendium (Lee 2025).

Table 2a. Correlations computed in this study. p values are descriptive (section 2.2). Data: NOAA CPC (ONI, NAO, AO, QBO50), NOAA PSL (QBO30); accessed 28 August 2026.

#	Pair	Period	***n***	***r***	***p***	Note
1	ONI(DJF) × NAO(DJF)	1951–2026	76	−0.04	0.74	The seasonal mean masks the relationship
2	ONI(DJF) × NAO(Nov–Dec)	1951–2026	76	+0.21	0.06	Early winter: positive tendency
3	ONI(DJF) × NAO(Jan–Mar)	1951–2026	76	−0.12	0.32	Late winter: reversal toward negative
4	ONI(DJF) × AO(DJF)	1951–2026	76	−0.12	0.30	
5	ONI(DJF) × AO(Jan–Mar)	1951–2026	76	−0.17	0.14	Strengthens in late winter
6	QBO50(ND) × AO(DJF)	1980–2026	47	−0.01	0.94	No surface imprint of Holton–Tan in the seasonal mean
7	QBO50(ND) × NAO(DJF)	1980–2026	47	+0.11	0.46	
8	QBO30(ND) × AO(DJF)	1951–2026	76	+0.06	0.59	Sign in the Holton–Tan direction but negligible
9	ONI(DJF) × U10–60N	1959–2024	66	−0.17	0.16	Vortex-level signature of the simple saturation scenario (Figure 7)
10	RONI(DJF) × U10–60N	1959–2024	66	−0.16	0.19	

Table 2b. Published coefficients (for comparison).

Source	Quantity	Value
Watson and Gray (2014, JAS)	QBO(50 hPa, Nov–Feb) × U(10 hPa, 60°N)	r = 0.58
Scaife et al. (2014, GRL)	GloSea5 ensemble mean × observed DJF NAO	r = 0.62
Butler and Polvani (2011, GRL)	SSW frequency, ENSO / neutral	~2×
Palmeiro et al. (2023, JGR)	SSW per decade: neutral 9.2, EN 8.3, LN 8.2 (1950–2021)	difference not significant
Baltacı et al. (2018, TAC)	AO × western Anatolian winter precipitation	r ≈ −0.5
Baltacı et al. (2018, TAC)	AO × Black Sea / Aegean warm days	r = −0.6 / −0.7
Türkeş and Erlat (2008, TAC)	AO × Türkiye mean winter temperature	negative, regionally variable
Mitchell et al. (2013, J. Climate)	Eurasian surface T anomaly after splits	up to −3 K

Table 3a. SSW frequency by ENSO phase, 1958–2024 (67 winters; events: compendium + 2024×2). The ENSO phase is defined by ONI_DJF. The last column is not a chronological per-decade rate but the descriptive equivalent of the total number of events scaled to 10 winters by the number of phase-winters (events per 10 phase-winters).

Phase	No. of winters	Winters with ≥1 SSW	Events	Events per 10 phase-winters
El Niño	24	14 (58%)	19	7.9
La Niña	23	15 (65%)	17	7.4
Neutral	20	9 (45%)	11	5.5

Table 3b. Sensitivity of winter-based SSW risk to the QBO phase definition. Outcome: at least one major SSW within the winter. Intervals are Clopper–Pearson exact 95% intervals; the risk ratio interval is computed on the log scale and p is Fisher's exact test.

QBO definition	Period	eQBO: ≥1 SSW	wQBO: ≥1 SSW	Risk ratio (95% CI)	**Fisher *p***
50 hPa November (main)	1980–2024	12/19 = 63% [38–84]	13/26 = 50% [30–70]	1.26 (0.75–2.12)	0.545
50 hPa November–December	1980–2024	12/19 = 63%	13/26 = 50%	1.26 (0.75–2.12)	0.545
50 hPa DJF (upper bound)	1980–2024	15/21 = 71%	10/24 = 42%	1.71 (0.99–2.96)	0.071
30 hPa November	1980–2024	16/25 = 64%	9/20 = 45%	1.42 (0.81–2.51)	0.239
30 hPa November (long record)	1958–2024	24/36 = 67% [49–81]	14/31 = 45% [27–64]	1.48 (0.94–2.32)	0.089

Table 3c. ENSO × QBO cells, winter-based risk (QBO phase = November 50 hPa; 1980–2024). Intervals are Clopper–Pearson exact; the last column is not a chronological time rate but the complementary event density scaled per 10 phase-winters.

Cell	Winter	≥1 SSW	Rate	95% exact CI	Events	Events per 10 phase-winters
La Niña × eQBO	6	5	0.83	0.36–1.00	6	10.0
La Niña × wQBO	10	7	0.70	0.35–0.93	7	7.0
Neutral × eQBO	7	4	0.57	0.18–0.90	5	7.1
Neutral × wQBO	6	1	0.17	0.00–0.64	2	3.3
El Niño × eQBO	6	3	0.50	0.12–0.88	4	6.7
El Niño × wQBO	10	5	0.50	0.19–0.81	7	7.0

Stratified Fisher's exact tests: La Niña p=1.000; neutral p=0.266 (odds ratio 6.67); El Niño p=1.000 (odds ratio 1.00). Firth penalized logistic model (ssw ~ eQBO + El Niño + eQBO×El Niño; n=45): odds ratio 2.11 for eQBO (95% CI 0.46–9.67) and 0.47 for the interaction (0.04–5.96), with a profile penalized LRT p=0.541. When the same model is built with the 30-hPa November phase and the 1958–2024 record (n=67), the collapse in the El Niño cells disappears (eQBO 9/13 = 0.69; wQBO 5/11 = 0.45) and the interaction odds ratio returns to 1.13 (0.14–8.92; p=0.904): the interaction cannot be resolved with the present sample.

Appendix A — Sensitivity to Threshold, Index and Definition

Table A1. Sensitivity of the super–wQBO pattern to the ONI threshold (1951–2024 catalog). The QBO phase is constructed with the main definition of the paper, the sign of the 50-hPa November mean; for winters before 1979 (1957/58, 1972/73) the CPC 50-hPa series is unavailable, so the phase is derived from the 30-hPa November mean and marked with ‡ in the table. SSW = at least one major event within the winter.

Threshold (ONI_DJF)	No. of winters	wQBO	**eQBO**	Winters with an SSW	Pattern
≥ +1.5	7	4	3	1957/58 (W‡), 1972/73 (E‡), 2023/24 (E)	mixed
≥ +1.8	4	3	1	2023/24 (E)	all wQBO winters SSW-free
≥ +2.0	3	3	0	—	pure: 3/3 wQBO and SSW-free

Reading: the pure form of the pattern appears only at the ≥+2.0 threshold; when the threshold is lowered to +1.5, both the strong easterly-QBO winters (1972/73 and 2023/24, each with an SSW) and 1957/58, which produced an SSW under westerly QBO, enter the table and the pattern becomes mixed. Because the threshold table is built with the main phase definition, it is directly comparable with the 50-hPa November and 30-hPa November rows of Table A3. This sensitivity is an independent justification for keeping the proposition of section 5 at the status of a hypothesis.

Table A2. Comparison of the ONI and RONI rulers (winters satisfying ONI_DJF ≥ +1.5 or RONI_DJF ≥ +1.5; RONI: CPC relative ONI, accessed 28 Aug 2026).

Winter	**ONI (DJF)**	**RONI (DJF)**	QBO50 (Nov)	QBO30 (Nov)	Major midwinter SSW
1957/58	+1.7	+1.89	—	W	Yes

Winter	**ONI (DJF)**	**RONI (DJF)**	QBO50 (Nov)	QBO30 (Nov)	Major midwinter SSW
1965/66	+1.2	+1.53	—	E	Yes
1972/73	+1.6	+1.69	—	E	Yes
1982/83	+2.1	+2.40	W	W	No
1991/92	+1.5	+2.12	E	E	No
1997/98	+2.2	+2.13	W	W	No
2015/16	+2.5	+2.14	W	W	No
2023/24	+1.8	+1.13	E	E	Yes (two events)

Reading: the RONI≥+2.0 set comprises four winters, all four of them free of a major midwinter SSW; the change of ruler from ONI to RONI extends the SSW-free component from 3/3 to 4/4. Phase purity, by contrast, weakens: 1991/92 is eQBO and the wQBO share falls to 3/4. This comparison shows that the SSW-free pattern and the wQBO conditioning hypothesis are not equally robust to a change of index. While 2023/24 approaches the super threshold in ONI, it falls back markedly in RONI.

Table A3. Sensitivity of the super–wQBO pattern to the QBO phase definition. Each cell gives, in order, the number of westerly-QBO winters, the number of easterly-QBO winters, and the number of winters with at least one major SSW among the winters satisfying the corresponding ONI threshold; the sum of the first two numbers equals the number of winters that can be classified at that threshold.

QBO definition	**ONI ≥ +2.0 (n=3)**	**ONI ≥ +1.8 (n=4)**	**ONI ≥ +1.5 (n=7)**
50 hPa November	3 / 0 / 0	3 / 1 / 1	3 / 2 / 3 (two winters unclassifiable†)
50 hPa November–December	3 / 0 / 0	3 / 1 / 1	3 / 2 / 3 (two winters unclassifiable†)
50 hPa DJF	3 / 0 / 0	3 / 1 / 1	3 / 2 / 3 (two winters unclassifiable†)
30 hPa November	3 / 0 / 0	3 / 1 / 1	4 / 3 / 3
30 hPa DJF	2 / 1 / 0	2 / 2 / 1	3 / 4 / 3

† For 1957/58 and 1972/73 the CPC 50-hPa series does not extend before 1979, so these two winters can be classified only in the 30-hPa rows.

Reading: at the ONI ≥ +2.0 threshold the 3/3 westerly-QBO pattern is preserved in the three 50-hPa windows and under 30-hPa November; only the 30-hPa DJF definition moves 1997/98 to the easterly side. When the threshold is lowered to +1.5 the pattern becomes mixed under every definition.

Appendix B — Split/Displacement Surface Composites

Table B1. Surface signatures compiled from the literature (to be read together with the caveats discussed in section 6).

Surface signature	Split (S)	Displacement (D)	Source
Eurasian surface temperature	cooling of up to −3 K	markedly weaker	Mitchell et al. (2013)
Eastern North America	warming exceeding +1.5 K	cooling of about −1.5 K	Mitchell et al. (2013)
Timing of surface descent	about 1 week earlier; immediate and barotropic	lagged by 1–2 weeks	Seviour et al. (2013); Hall et al. (2021); White et al. (2021)
NAO/NAM signature difference	small	small	Hall et al. (2021)
After 3–4 weeks	no difference	no difference	White et al. (2021); Maycock and Hitchcock (2015)
Statistical status	significant in reanalysis, not in large ensembles	—	Charlton and Polvani (2007); Lehtonen and Karpechko (2016); White et al. (2019)

Appendix C — Details of the Vortex–Türkiye Regression (ERA5)

This appendix gives the full coefficient table of the ERA5 regional regression summarized in section 7.1 together with the ND/JFM maps not included in the main text. The design, data and uncertainty method are defined in section 2.2; in all five boxes the area mean is cosine-latitude weighted and taken without a land–sea mask; all values are per +1 standard deviation of DJF U10–60N, and for weak-vortex winters the signs reverse symmetrically.

Table C1. Grid-level significance summary: fraction of grid cells with local $p<0.05$, fraction passing BH-FDR ($\alpha=0.10$), and the correlation of the DJF-predictor pattern with the concurrent-predictor pattern (conc_r; an indicator of acausality for ND).

Window	Variable	Local % <0.05	% passing FDR	**conc_r**
DJF	Z500	42.0	36.6	1.00
DJF	Precipitation	12.4	1.5	1.00
DJF	T2m	17.9	2.0	1.00
ND	Z500	18.8	16.6	0.68
ND	Precipitation	7.9	0.0	0.55
ND	T2m	10.7	0.0	0.47
JFM	Z500	34.6	25.4	0.96
JFM	Precipitation	10.9	1.0	0.90
JFM	T2m	19.0	6.5	0.91

Table C2. Regional mean precipitation coefficients (mm month^{-1} per +1 sd U10–60N; winter-based bootstrap 95% CI); the regional means are cosine-latitude-weighted full-area means taken without a land–sea mask. Model A: U10 only; Model B: U10 + concurrent NAO; Indirect = bootstrap distribution of the A − B difference. Concurrent U10–NAO correlation: DJF r=+0.41, ND +0.10, JFM +0.45.

Window	Region	Model A β [95% CI]	% clim.	**Model B β**	Indirect (A−B) [95% CI]
DJF	Türkiye	−5.49 [−10.47, −0.83]	−6.8	−5.28	−0.14 [−2.34, +1.82]
DJF	Marmara	−5.46 [−10.90, −0.22]	−6.9	−4.61	−0.65 [−4.65, +2.24]
DJF	Aegean	−9.69 [−17.81, −1.60]	−10.0	−8.50	−0.99 [−6.34, +3.38]
DJF	Mediterranean coast	−8.79 [−19.29, +1.53]	−8.1	−8.97	+0.15 [−3.70, +4.82]
DJF	Levant	−2.79 [−8.62, +3.08]	−4.0	−3.13	+0.28 [−1.47, +2.50]
ND	Türkiye	−4.28 [−10.91, +2.30]	−5.7	−4.00	−0.18 [−2.42, +0.71]
ND	Marmara	−3.50 [−12.92, +6.02]	−4.4	−2.71	−0.66 [−3.90, +1.74]
ND	Aegean	−4.27 [−16.19, +5.85]	−4.8	−3.12	−1.10 [−5.93, +2.10]
ND	Mediterranean coast	−11.89 [−24.72, −0.55]	−12.1	−10.95	−0.81 [−5.10, +1.72]
ND	Levant	−6.55 [−12.89, −0.37]	−11.1	−6.51	−0.03 [−1.29, +0.74]
JFM	Türkiye	−2.25 [−6.67, +1.72]	−2.9	+0.10	−2.18 [−5.46, −0.14]
JFM	Marmara	−3.26 [−8.55, +1.57]	−4.5	+1.04	−4.11 [−8.56, −0.73]
JFM	Aegean	−5.72 [−12.86, +1.21]	−6.5	−1.82	−3.75 [−9.34, +0.14]
JFM	Mediterranean coast	−2.41 [−10.29, +5.17]	−2.7	−0.43	−1.86 [−7.75, +2.56]
JFM	Levant	−0.27 [−4.83, +3.79]	−0.5	−0.28	0.00 [−2.68, +2.70]

Reading: in the DJF rows all five regions give negative coefficients and three of them exclude zero; in ND the signal shifts to the southern coastal belt; in JFM all intervals include zero and, while controlling for the NAO erases the coefficients, the indirect component moves away from zero. The table collects the three findings of section 7.1 — a consistent but modest dry-signed link in midwinter, the shift of the calendar, and the window dependence of the role of the NAO — in a single ledger. The ND rows should be read more cautiously than the others because of the partial acausality of the DJF predictor with respect to the ND response (conc_r=0.68 in Table C1). When the fifteen Model-A coefficients of Table C2 are treated as a single family under BH-FDR ($\alpha=0.10$), none passes the threshold (smallest p=0.022, DJF Türkiye box); individual intervals that exclude zero are exploratory signals.

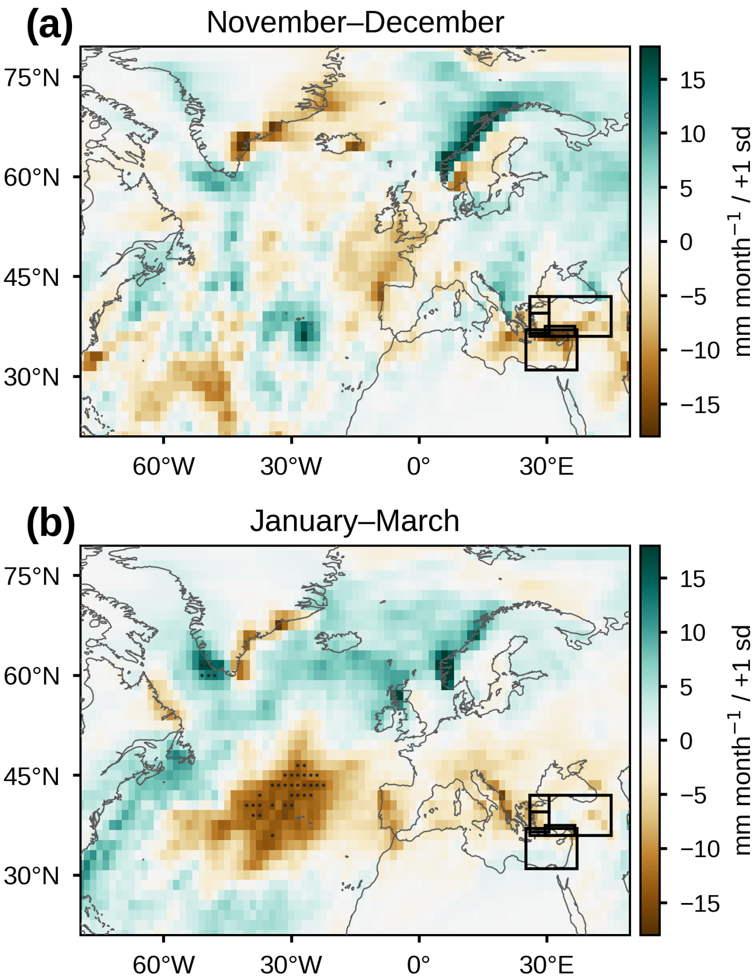

Figure C1. The ND (top) and JFM (bottom) counterparts of Figure 9: precipitation coefficient maps (mm month^{-1} per +1 sd DJF U10–60N) and the regional boxes; the stippling follows the same criterion as in Figure 9, and the boxes are full-area means without a land–sea mask. The ND panels are built with the DJF predictor and are partly acausal (pattern correlation with the concurrent predictor 0.68); in the JFM panel no regional interval excludes zero. The data identification is the same as in Figure 9. Quantitative figure.

Reproducibility Correction

During the reproducibility audit we determined that the regional box-average convention had been described incorrectly in the methods text. The printed coefficients were verified to have been produced from cosine-latitude-weighted full-area means without a land–sea mask, and the description of the method (sections 2.2 and 9 and Appendix C) was corrected accordingly. None of the numerical results changed.

Use of Generative AI Tools

Generative artificial intelligence tools were used as an auxiliary aid in the conceptual visualization of the study and the development of the figure design, in cross-checking code and calculations, and in verifying table–text consistency. Figures 1–6 are conceptual drawings reconstructed in vector form and are not quantitative data maps; Figures 7–9 and Figure C1 were produced directly from data series and fields. All numerical results were computed from publicly available data series with the scripts published in the supplement, and AI outputs were not used as independent data or as scientific evidence.

Data Availability Statement

All series used are publicly available: ONI and RONI (NOAA CPC, ERSSTv6), the monthly NAO and AO indices (CPC), the 50-hPa equatorial zonal wind (CPC/CDAS), the 30-hPa QBO series (NOAA PSL), the 10-hPa 60°N zonal-mean wind (NCEP/NCAR Reanalysis-1; NOAA PSL) and the major SSW event catalog (NOAA CSL SSW Compendium; Butler et al. 2017), with Lee (2025) for the 2023/24 events. The monthly Z500, total precipitation and 2-m temperature fields used in the regional analysis are taken from the 1.5° monthly ERA5 derivative distributed through the WeatherBench2 channel (Hersbach et al. 2020; Rasp et al. 2024); these fields were accessed on 29 August 2026 and all other series on 28 August 2026. The winter-based catalog, the derived frequency tables, and all scripts producing the bootstrap, Fisher and Firth calculations and Figures 7–9 and Figure C1 have been prepared for publication in a permanent archive together with data access dates and version identifications; the archive will be published on Zenodo before submission and the DOI will be entered in this statement (doi:10.5281/zenodo.⟨reservation pending⟩; version v1.1, 2026). The repository has been prepared to include not only the code but also access-dated snapshots of the downloaded ONI, RONI, NAO, AO, QBO, SSW and ERA5 files, product version identifications, and a step-by-step reproduction guide in the README; all values in Tables 1, 2a and 3a–3c, in Appendices A and B and in Appendix C can be reproduced from the raw series and fields.

References

Anstey, J. A., and T. G. Shepherd, 2014: High-latitude influence of the quasi-biennial oscillation. Quart. J. Roy. Meteor. Soc., 140, 1–21, doi:10.1002/qj.2132.

Baldwin, M. P., and T. J. Dunkerton, 2001: Stratospheric harbingers of anomalous weather regimes. Science, 294, 581–584, doi:10.1126/science.1063315.

Baldwin, M. P., and Coauthors, 2021: Sudden stratospheric warmings. Rev. Geophys., 59, e2020RG000708, doi:10.1029/2020RG000708.

Baltacı, H., B. O. Akkoyunlu, and M. Tayanç, 2018: Relationships between teleconnection patterns and Turkish climatic extremes. Theor. Appl. Climatol., 134, 1365–1386, doi:10.1007/s00704-017-2350-z.

Barriopedro, D., and N. Calvo, 2014: On the relationship between ENSO, stratospheric sudden warmings, and blocking. J. Climate, 27, 4704–4720, doi:10.1175/jcli-d-13-00770.1.

Barton, C. A., and J. P. McCormack, 2017: Origin of the 2016 QBO disruption and its relationship to extreme El Niño events. Geophys. Res. Lett., 44, 11 150–11 157, doi:10.1002/2017GL075576.

Bell, C. J., L. J. Gray, A. J. Charlton-Perez, M. M. Joshi, and A. A. Scaife, 2009: Stratospheric communication of El Niño teleconnections to European winter. J. Climate, 22, 4083–4096, doi:10.1175/2009jcli2717.1.

Benjamini, Y., and Y. Hochberg, 1995: Controlling the false discovery rate: A practical and powerful approach to multiple testing. J. Roy. Statist. Soc., 57B, 289–300.

Butler, A. H., and L. M. Polvani, 2011: El Niño, La Niña, and stratospheric sudden warmings: A reevaluation in light of the observational record. Geophys. Res. Lett., 38, L13807, doi:10.1029/2011GL048084.

Butler, A. H., D. J. Seidel, S. C. Hardiman, N. Butchart, T. Birner, and A. Match, 2015: Defining sudden stratospheric warmings. Bull. Amer. Meteor. Soc., 96, 1913–1928, doi:10.1175/bams-d-13-00173.1.

Butler, A. H., J. P. Sjoberg, D. J. Seidel, and K. H. Rosenlof, 2017: A sudden stratospheric warming compendium. Earth Syst. Sci. Data, 9, 63–76, doi:10.5194/essd-9-63-2017.

Cagnazzo, C., and E. Manzini, 2009: Impact of the stratosphere on the winter tropospheric teleconnections between ENSO and the North Atlantic and European region. J. Climate, 22, 1223–1238, doi:10.1175/2008jcli2549.1.

Calvo, N., M. A. Giorgetta, R. Garcia-Herrera, and E. Manzini, 2009: Nonlinearity of the combined warm ENSO and QBO effects on the Northern Hemisphere polar vortex in MAECHAM5 simulations. J. Geophys. Res., 114, D13109, doi:10.1029/2008jd011445.

Charlton, A. J., and L. M. Polvani, 2007: A new look at stratospheric sudden warmings. Part I: Climatology and modeling benchmarks. J. Climate, 20, 449–469, doi:10.1175/jcli3996.1.

Coy, L., P. A. Newman, S. Pawson, and L. R. Lait, 2017: Dynamics of the disrupted 2015/16 quasi-biennial oscillation. J. Climate, 30, 5661–5674, doi:10.1175/jcli-d-16-0663.1.

Domeisen, D. I. V., C. I. Garfinkel, and A. H. Butler, 2019: The teleconnection of El Niño Southern Oscillation to the stratosphere. Rev. Geophys., 57, 5–47, doi:10.1029/2018rg000596.

Dunkerton, T. J., D. P. Delisi, and M. P. Baldwin, 1988: Distribution of major stratospheric warmings in relation to the quasi-biennial oscillation. Geophys. Res. Lett., 15, 136–139, doi:10.1029/gl015i002p00136.

Ebdon, R. A., 1975: The quasi-biennial oscillation and its association with tropospheric circulation patterns. Meteor. Mag., 104, 282–297.

Garfinkel, C. I., and D. L. Hartmann, 2008: Different ENSO teleconnections and their effects on the stratospheric polar vortex. J. Geophys. Res., 113, D18114, doi:10.1029/2008jd009920.

Garfinkel, C. I., A. H. Butler, D. W. Waugh, M. M. Hurwitz, and L. M. Polvani, 2012a: Why might stratospheric sudden warmings occur with similar frequency in El Niño and La Niña winters? J. Geophys. Res., 117, D19106, doi:10.1029/2012JD017777.

Garfinkel, C. I., T. A. Shaw, D. L. Hartmann, and D. W. Waugh, 2012b: Does the Holton–Tan mechanism explain how the quasi-biennial oscillation modulates the Arctic polar vortex? J. Atmos. Sci., 69, 1713–1733, doi:10.1175/JAS-D-11-0209.1.

Geng, X., W. Zhang, M. F. Stuecker, and F.-F. Jin, 2017: Strong sub-seasonal wintertime cooling over East Asia and Northern Europe associated with super El Niño events. Sci. Rep., 7, 3770, doi:10.1038/s41598-017-03977-2.

Gray, L. J., J. A. Anstey, Y. Kawatani, H. Lu, S. Osprey, and V. Schenzinger, 2018: Surface impacts of the quasi biennial oscillation. Atmos. Chem. Phys., 18, 8227–8247, doi:10.5194/acp-18-8227-2018.

Hall, R. J., D. M. Mitchell, W. J. M. Seviour, and C. J. Wright, 2021: Tracking the stratosphere-to-surface impact of sudden stratospheric warmings. J. Geophys. Res. Atmos., 126, e2020JD033881, doi:10.1029/2020jd033881.

Hersbach, H., and Coauthors, 2020: The ERA5 global reanalysis. Quart. J. Roy. Meteor. Soc., 146, 1999–2049, doi:10.1002/qj.3803.

Holton, J. R., and H.-C. Tan, 1980: The influence of the equatorial quasi-biennial oscillation on the global circulation at 50 mb. J. Atmos. Sci., 37, 2200–2208, doi:10.1175/1520-0469(1980)037<2200:tioteq>2.0.co;2.

Ineson, S., and A. A. Scaife, 2009: The role of the stratosphere in the European climate response to El Niño. Nat. Geosci., 2, 32–36, doi:10.1038/ngeo381.

Kalnay, E., and Coauthors, 1996: The NCEP/NCAR 40-year reanalysis project. Bull. Amer. Meteor. Soc., 77, 437–471, doi:10.1175/1520-0477(1996)077<0437:TNYRP>2.0.CO;2.

Karpechko, A. Yu., P. Hitchcock, D. H. W. Peters, and A. Schneidereit, 2017: Predictability of downward propagation of major sudden stratospheric warmings. Quart. J. Roy. Meteor. Soc., 143, 1459–1470, doi:10.1002/qj.3017.

Kömüşcü, A. Ü., and K. Oğuz, 2021: Analysis of cold anomalies observed over Turkey during the 2018/2019 winter in relation to polar vortex and other atmospheric patterns. Meteor. Atmos. Phys., 133, 1327–1354, doi:10.1007/s00703-021-00806-0.

Krichak, S. O., P. Kishcha, and P. Alpert, 2002: Decadal trends of main Eurasian oscillations and the eastern Mediterranean precipitation. Theor. Appl. Climatol., 72, 209–220, doi:10.1007/s007040200021.

Kumar, V., S. Yoden, and M. H. Hitchman, 2022: QBO and ENSO effects on the mean meridional circulation, polar vortex, subtropical westerly jets, and wave patterns during boreal winter. J. Geophys. Res. Atmos., 127, e2022JD036691, doi:10.1029/2022jd036691.

Lee, S. H., 2025: Two major sudden stratospheric warmings during winter 2023/2024. Weather, 80, 45–53, doi:10.1002/wea.7656.

Lehtonen, I., and A. Yu. Karpechko, 2016: Observed and modeled tropospheric cold anomalies associated with sudden stratospheric warmings. J. Geophys. Res. Atmos., 121, 1591–1610, doi:10.1002/2015JD023860.

Lu, H., M. H. Hitchman, L. J. Gray, J. A. Anstey, and S. M. Osprey, 2020: On the role of Rossby wave breaking in the quasi-biennial modulation of the stratospheric polar vortex during boreal winter. Quart. J. Roy. Meteor. Soc., 146, 1939–1959, doi:10.1002/qj.3775.

Manzini, E., and Coauthors, 2024: Nonlinearity and asymmetry of the ENSO stratospheric pathway to North Atlantic and Europe, revisited. J. Geophys. Res. Atmos., 129, e2023JD039992, doi:10.1029/2023jd039992.

Marshall, A. G., and A. A. Scaife, 2009: Impact of the QBO on surface winter climate. J. Geophys. Res., 114, D18110, doi:10.1029/2009jd011737.

Maycock, A. C., and P. Hitchcock, 2015: Do split and displacement sudden stratospheric warmings have different annular mode signatures? Geophys. Res. Lett., 42, 10943–10951, doi:10.1002/2015gl066754.

Mitchell, D. M., L. J. Gray, J. Anstey, M. P. Baldwin, and A. J. Charlton-Perez, 2013: The influence of stratospheric vortex displacements and splits on surface climate. J. Climate, 26, 2668–2682, doi:10.1175/jcli-d-12-00030.1.

Nakagawa, K. I., and K. Yamazaki, 2006: What kind of stratospheric sudden warming propagates to the troposphere? Geophys. Res. Lett., 33, L04801, doi:10.1029/2005gl024784.

Newman, P. A., L. Coy, S. Pawson, and L. R. Lait, 2016: The anomalous change in the QBO in 2015–2016. Geophys. Res. Lett., 43, 8791–8797, doi:10.1002/2016gl070373.

Osprey, S. M., N. Butchart, J. R. Knight, A. A. Scaife, K. Hamilton, J. A. Anstey, V. Schenzinger, and C. Zhang, 2016: An unexpected disruption of the atmospheric quasi-biennial oscillation. Science, 353, 1424–1427, doi:10.1126/science.aah4156.

Palmeiro, F. M., and Coauthors, 2023: On the influence of ENSO on sudden stratospheric warmings. J. Geophys. Res. Atmos., 128, e2022JD037607, doi:10.1029/2022jd037607.

Rasp, S., and Coauthors, 2024: WeatherBench 2: A benchmark for the next generation of data-driven global weather models. J. Adv. Model. Earth Syst., 16, e2023MS004019, doi:10.1029/2023MS004019.

Ren, R.-C., and Coauthors, 2017: Parallel comparison of the 1982/83, 1997/98 and 2015/16 super El Niños and their effects on the extratropical stratosphere. Adv. Atmos. Sci., 34, 1121–1133, doi:10.1007/s00376-017-6260-x.

Richter, J. H., K. Matthes, N. Calvo, and L. J. Gray, 2011: Influence of the quasi-biennial oscillation and El Niño–Southern Oscillation on the frequency of sudden stratospheric warmings. J. Geophys. Res., 116, D20111, doi:10.1029/2011jd015757.

Scaife, A. A., and Coauthors, 2014: Skillful long-range prediction of European and North American winters. Geophys. Res. Lett., 41, 2514–2519, doi:10.1002/2014gl059637.

Seviour, W. J. M., D. M. Mitchell, and L. J. Gray, 2013: A practical method to identify displaced and split stratospheric polar vortex events. Geophys. Res. Lett., 40, 5268–5273, doi:10.1002/grl.50927.

Sezen, C., and T. Partal, 2019: The impacts of Arctic oscillation and the North Sea Caspian pattern on the temperature and precipitation regime in Turkey. Meteor. Atmos. Phys., 131, 1677–1696, doi:10.1007/s00703-019-00665-w.

Trigo, R. M., and Coauthors, 2006: Relations between variability in the Mediterranean region and mid-latitude variability. Mediterranean Climate Variability, P. Lionello et al., Eds., Elsevier, 179–226, doi:10.1016/s1571-9197(06)80006-6.

Türkeş, M., and E. Erlat, 2003: Precipitation changes and variability in Turkey linked to the North Atlantic Oscillation during the period 1930–2000. Int. J. Climatol., 23, 1771–1796, doi:10.1002/joc.962.

Türkeş, M., and E. Erlat, 2008: Influence of the Arctic Oscillation on variability of winter mean temperatures in Turkey. Theor. Appl. Climatol., 92, 75–85, doi:10.1007/s00704-007-0310-8.

Watson, P. A. G., and L. J. Gray, 2014: How does the quasi-biennial oscillation affect the stratospheric polar vortex? J. Atmos. Sci., 71, 391–409, doi:10.1175/jas-d-13-096.1.

Wei, K., W. Chen, and R. Huang, 2007: Association of tropical Pacific sea surface temperatures with the stratospheric Holton–Tan oscillation in the Northern Hemisphere winter. Geophys. Res. Lett., 34, L16814, doi:10.1029/2007gl030478.

White, I. P., and Coauthors, 2019: The downward influence of sudden stratospheric warmings: Association with tropospheric precursors. J. Climate, 32, 85–108, doi:10.1175/jcli-d-18-0053.1.

White, I. P., and Coauthors, 2021: The impact of split and displacement sudden stratospheric warmings on the troposphere. J. Geophys. Res. Atmos., 126, e2020JD033989, doi:10.1029/2020jd033989.

Wilks, D. S., 2016: "The stippling shows statistically significant grid points": How research results are routinely overstated and overinterpreted, and what to do about it. Bull. Amer. Meteor. Soc., 97, 2263–2273, doi:10.1175/BAMS-D-15-00267.1.

Zhang, C., J. Zhang, X. Xia, and D. Li, 2024: Impact of Arctic stratospheric polar vortex on Mediterranean precipitation. J. Climate, 37, 4403–4419, doi:10.1175/JCLI-D-23-0469.1.

Zhou, X., Q. Chen, F. Xie, J. Li, M. Li, R. Ding, Y. Li, X. Xia, and Z. Cheng, 2019: Nonlinear response of the Northern Hemisphere stratospheric polar vortex to the Indo–Pacific warm pool (IPWP) Niño. Sci. Rep., 9, 13719, doi:10.1038/s41598-019-49449-7.